Theoretical investigation of microstructure evolution and deformation of zirconium under neutron irradiation

A.V. Barashev[a,b*], S.I. Golubov[a] and R.E. Stoller[a]

[a] Materials Science and Technology Division, ORNL, Oak Ridge, TN 37831- 6138, USA
[b] Center for Materials Processing, Department of Materials Science and Engineering, University of Tennessee, East Stadium Hall, Knoxville, TN 37996-0750, USA

Abstract

This paper is a theoretical study of the dose dependence of radiation growth of zirconium using the reaction-diffusion model proposed recently in [1] and [2]. In the model, the strain rates are functions of the dislocation densities, which include contribution from dislocation loops, and the spatial distribution of their Burgers vectors. The model takes into account the intra-cascade clustering of self-interstitial atoms and their one-dimensional diffusion; explains the growth stages, including the break-away growth of pre-annealed samples; and accounts for such striking observations as negative strain in prismatic direction, and co-existence of vacancy- and interstitial-type prismatic loops. In this paper, the change of dislocation density due to accumulation of sessile dislocation loops during irradiation is taken into account explicitly. The the model is fitted to available experimental data and numerical calculations of the strain behavior of Zr for different initial dislocation structures are presented. The effect of cold work and the role of vacancy loops in the strain behavior are elucidated, and the maximum strain rates are estimated. The strains at large irradiation doses are predicted to increase linearly with dose increasing with a rate determined by the ratio of basal and prismatic loop densities. The dislocation climb velocities are calculated, which are important for the 'climb-induced glide' model of creep.

Key words: radiation growth, hcp metals, neutron irradiation, theory, displacement cascades.

PACS codes: 61.80.Az.; 61.80.Hg., 61.82.Bg.

*Corresponding author. *Email address*: abarashe@utk.edu (A.V. Barashev).

1. Introduction

The radiation growth (RG) of Zr-based materials with the hexagonal close-packed (hcp) crystal lattices is one of the damaging mechanisms which affect safe and economical operation of commercial nuclear reactors. Several theoretical models of RG have been published since the first model by Buckley about a half of a century ago [3] (see [4] for a review). All of them (with one exception discussed below) were based on the Standard Rate Theory, where the primary damage is in the form of Frenkel pairs, i.e. single vacancies and self-interstitial atoms (SIAs), both migrating three-dimensionally (3-D), so that many important observations remained Most significant step in understanding RG was made by Woo and Gösele [5] and [6] by introducing anisotropic diffusion of SIAs. In the diffusion anisotropy difference (DAD) model [6] it was assumed that the vacancy diffusion is isotropic, whereas the SIAs migrate preferentially along the basal planes. This allowed explaining the contraction of *c* axes and the crucial role of *c* loops in the breakaway stage in annealed Zr crystals.

Nevertheless, we argue that the DAD model does not describe correctly the RG in neutron-irradiated materials. This is because it assumes that the primary damage consists of Frenkel pairs, i.e. single vacancies and SIAs, only, whereas experiments (see, e.g. [7]) and molecular dynamics (MD) simulations (see [8] and, e.g. [9] for a recent review) show that a large fraction, ~20-50%, of defects are produced in the clustered form. The SIA clusters are highly mobile and migrate one-dimensionally (1-D) along close-packed directions in all crystals including Zr [8] and [10]. This lead to a mixture of second-order (for the point defects (PDs)) and third-order (for the SIA clusters) reaction kinetics [11], rather than just second order, as in the DAD model. Holt *et al.* [12] made an attempt to generalize the model by accounting for the cascade-produced SIA clusters, but assumed the clusters to be immobile, which was also incorrect. Another failure of these works is that they do not explain the co-existence of vacancy and interstitial loops, which is often observed in irradiated samples.

Recently we have proposed a reaction-diffusion model of RG [1] and [2], which is based on the Production Bias Model (PBM) [13], [14], [15] and [16]. The PBM represents a significant step in development of the theory of void swelling in materials with cubic lattices. The predictions of the PBM are consistent with a broad range of experimental results. It accounts for such observations as enhanced swelling near grain boundaries and void-lattice formation, which could not be explained by earlier models. This success is due to inclusion of the cascade production and 1-D migration of SIA clusters (small interstitial-type dislocation loops) into the theory.

The displacement cascades in hcp Zr are similar to those in cubic crystals; hence the PBM may provide a realistic framework for the hcp metals as well. Also, the basal-plane alignment of vacancy loops [17] and [18] and voids [19], which are observed in hcp metals irradiated at low and high temperature, respectively, is analogous to void ordering in cubic metals. Such a similarity gives additional support to the idea that, with certain modifications accounting for the features of hcp lattice, the PBM will be capable of describing RG.

The model proposed in [1] and [2] reproduces the RG stages observed, including the break-away growth in pre-annealed samples at high irradiation doses, and accounts for such striking observations as negative strains in prismatic directions and co-existence of vacancy- and

interstitial-type prismatic loops, both of which are unexplainable in the framework of any model based on the assumption that Frenkel pairs are the only form of initial damage created by incident particles (see [2] for a more detailed critical analysis of these models). The model gives qualitative and quantitative description for the instantaneous strain rates for a given microstructure. Accumulation of vacancy and interstitial loops results in increase of the total dislocation densities, hence in the dose dependence of radiation growth rates. The description of this process is the main aim of the present work.

The paper is organized as follows. In Section 2, the model is described. In Section 3, selected calculations are presented, obtained using a computer code RIMD-ZR.V1 (Radiation Induced Microstructure and Deformation of Zr, Version 1) developed. A summary is given in Section 4.

2. The model

2.1. Basic assumptions

As in [1] and [2], the following framework is used:

1. Initial microstructure consists of *a*- and *c*-type edge dislocations; densities of dislocations with the Burgers vectors along $\mathbf{a_1}$, $\mathbf{a_2}$ and $\mathbf{a_3}$ prismatic directions, ρ_j, may be unequal.
2. Mobile PDs and SIA clusters are steadily produced in displacement cascades.
3. The PDs execute 3-D random walk, whereas SIA clusters migrate 1-D along their Burgers vectors, i.e. one of the $\langle 11\bar{2}0 \rangle$ directions, parallel to the basal planes.
4. The SIA clusters interact with dislocations of the same Burgers vector only, while the much weaker interaction with other dislocations is ignored (see analysis in [1] or [2]).
5. The dislocation bias factor for PDs, mutual recombination of PDs, and thermal-equilibrium vacancies are ignored.

2.2. Equations and fluxes of PDs and SIA clusters

In the framework formulated, the equations for concentrations, *C*, of mobile defects: single vacancies (subscript v), single SIAs (i) and glissile SIA clusters (cl) are as follows (here and then the following indexes are used: $j = \mathbf{a_1}, \mathbf{a_2}, \mathbf{a_3}, \mathbf{c}$ and $m = \mathbf{a_1}, \mathbf{a_2}, \mathbf{a_3}$):

$$\dot{C}_{\mathrm{v}} = G - \rho D_{\mathrm{v}} C_{\mathrm{v}}, \tag{1}$$

$$\dot{C}_{\mathrm{i}} = G\left(1 - \varepsilon_{\mathrm{i}}^{\mathrm{g}}\right) - \rho D_{\mathrm{i}} C_{\mathrm{i}}, \tag{2}$$

$$\dot{C}_{\mathrm{cl}}^{m} = G \frac{\varepsilon_{\mathrm{i}}^{\mathrm{g}}}{3 n_{\mathrm{i}}^{\mathrm{g}}} - k_m^2 D_{\mathrm{cl}} C_{\mathrm{cl}}^{m}, \tag{3}$$

where $G = G^{\mathrm{NRT}}(1 - \varepsilon_{\mathrm{r}})$, G^{NRT} being the NRT standard dose rate and ε_{r} the fraction of defects recombining in cascades; $\varepsilon_{\mathrm{i}}^{\mathrm{g}}$ is the fraction of SIAs produced in cascades in the clustered form;

$\rho = \sum_j \rho_j$ is the total density of edge dislocations and dislocation loops; D_{v} and D_{i} are the diffusion coefficients of a single vacancy and an SIA, respectively; $n_{\mathrm{i}}^{\mathrm{g}}$ is the mean number of SIAs in a cascade-produced glissile cluster; k_m^2 is the sink strength for the SIA clusters migrating along *m* direction, which is given by (see, e.g. [11] and [16])

$$k_m^2 = 2\left(\frac{\pi r_{\mathrm{cd}} \rho_m}{2}\right)^2, \tag{4}$$

where r_{cd} is the dislocation capture radius for glissile clusters. The factor 1/3 on the right-hand side (RHS) of Eq. (3) accounts for the equality of defect production rates in the three: $\mathbf{a_1}$, $\mathbf{a_2}$ and $\mathbf{a_3}$, prismatic directions. The first terms on the RHSs of Eqs. (1)-(3) account for the production of defects in cascades and the second terms for their loss at dislocations, including sessile loops.

Since the change in the concentrations of mobile defects happens at much higher rates than the changes in the sessile loop population, we use the steady-state fluxes of mobile species, which are found by setting the time derivatives in Eqs. (1)-(3) to zero:

$$D_{\mathrm{v}} C_{\mathrm{v}} = \frac{G}{\rho}, \tag{5}$$

$$D_{\mathrm{i}} C_{\mathrm{i}} = \left(1 - \varepsilon_{\mathrm{i}}^{\mathrm{g}}\right)\frac{G}{\rho}, \tag{6}$$

$$D_{\mathrm{cl}} C_{\mathrm{cl}}^m = \frac{1}{3 n_{\mathrm{i}}^{\mathrm{g}}} \frac{G \varepsilon_{\mathrm{i}}^{\mathrm{g}}}{k_m^2}. \tag{7}$$

2.3. Equations for strains

The following equations for the strain rates as functions of dislocations densities were derived in [1] and [2]. In a Cartesian coordinate system, where the *x* axis is along $\mathbf{a_1}$, *y* along $\mathbf{a_3}$-$\mathbf{a_2}$ and *z* along **c** directions, the strains, ε, evolve as $(i = \mathrm{x,y})$:

$$\frac{d\varepsilon_i}{d\phi} = \chi\left(\frac{1}{2} - \frac{\rho_i}{\rho}\right), \tag{8}$$

$$\frac{d\varepsilon_{\mathrm{z}}}{d\phi} = -\chi \frac{\rho_{\mathrm{z}}}{\rho}, \tag{9}$$

where $\phi = G^{\mathrm{NRT}} t$ is the irradiation dose, $\chi = \left(1 - \varepsilon_{\mathrm{r}}\right)\varepsilon_{\mathrm{i}}^{\mathrm{g}}$. In these equations

$$\rho_{\mathrm{x}} = \rho_{\mathrm{a}_1} + \left(\rho_{\mathrm{a}_2} + \rho_{\mathrm{a}_3}\right)\cos^2\left(\pi/3\right), \tag{10}$$

$$\rho_{\mathrm{y}} = \left(\rho_{\mathrm{a}_2} + \rho_{\mathrm{a}_3}\right)\sin^2\left(\pi/3\right), \tag{11}$$

$$\rho_{\mathrm{z}} = \rho_{\mathrm{c}}, \tag{12}$$

and describe effective dislocation densities in corresponding directions ($\rho_x + \rho_{\mathrm{y}} = \rho_{\mathrm{a}_1} + \rho_{\mathrm{a}_2} + \rho_{\mathrm{a}_3}$).

The dislocation densities include contributions from sessile dislocation loops of vacancy and interstitial type ($j = \mathbf{a_1}, \mathbf{a_2}, \mathbf{a_3}, \mathbf{c}$):

$$\rho_j = \rho_{\mathrm{d}}^j + 2\pi r_{\mathrm{v}}^j N_{\mathrm{v}}^j + 2\pi r_{\mathrm{i}}^j N_{\mathrm{i}}^j, \tag{13}$$

where ρ_{d}^j is the edge dislocation density, and $r_{\mathrm{v,i}}^j$ and $N_{\mathrm{v,i}}^j$ are the mean radius and number density of vacancy (subscript v) and interstitial (subscript i) loops of *j* orientation of the Burgers vector. The loops nucleate and grow or shrink via collisions with mobile SIA clusters and PDs in the course of irradiation. This leads to the dose dependence of dislocation densities and deformation rates, in accordance with Eqs. (8) and (9). To describe the dose dependence one needs the nucleation and growth scenarios, which are described in the following sections.

2.4. Nucleation of sessile loops

There is no fundamental information on the nucleation mechanisms of sessile dislocation loops in hcp metals, including Zr. For this reason, we use the following description, which reproduces the experimental observations:

1. Interstitial and vacancy prismatic loops are formed from the very beginning of irradiation, until reaching a maximum number densities, $N^{\mathrm{a,max}}$.
2. Basal vacancy loops nucleate after some critical dose, ϕ_0^{c}, until reaching a maximum number density, $N^{\mathrm{c,max}}$.
3. The nucleation of vacancy- or interstitial-type sessile loops takes place, if the net flux of corresponding defects, vacancies or SIAs, is positive.

To describe evolution of the loop number densities, we use the following equations.

$$\frac{dN^m}{d\phi} = \begin{cases} N^{\mathrm{a,max}}/3\phi_{\max}^{\mathrm{a}}, & N^m \le N^{\mathrm{a,max}}/3, \\ 0\,, & N^m \ge N^{\mathrm{a,max}}/3, \end{cases} \tag{14}$$

$$\frac{dN^{\mathrm{c}}}{d\phi} = \begin{cases} 0\,, & \phi < \phi_0^{\mathrm{c}}, \\ N^{\mathrm{c,max}} \dfrac{A\exp\left[A\left(\phi - \phi_0^{\mathrm{c}}\right)/\left(\phi_{\max}^{\mathrm{c}} - \phi_0^{\mathrm{c}}\right)\right]}{\left(\phi_{\max}^{\mathrm{c}} - \phi_0^{\mathrm{c}}\right)\left(\exp\left(A\right) - 1\right)}\,, & \phi \ge \phi_0^{\mathrm{c}}, N^{\mathrm{c}} < N^{\mathrm{c,max}}, \\ 0\,, & \phi \ge \phi_0^{\mathrm{c}}, N^{\mathrm{c}} \ge N^{\mathrm{c,max}}. \end{cases} \tag{15}$$

In these equations, A is a dimensionless parameter, and $\phi^{\mathrm{c}}_{\max}$ is the terminal dose for nucleation of basal vacancy-type loops. Parameter $\phi^{\mathrm{a}}_{\max}$ has the meaning of the terminal dose for nucleation of prismatic interstitial-type loops for isotropic distribution of prismatic dislocations. For non-isotropic distribution it is just a rate parameter defining nucleation of both vacancy- and interstitial-type prismatic loops.

2.5. Sessile dislocation loops

When nucleation process is characterized in details, the comprehensive description of the evolution of the population of sessile vacancy- and interstitial-type dislocation loops can be obtained from the Master equations in terms of the corresponding size-distribution functions. Then, generally a large number of equations is considered, one for each cluster size, which would require employing some grouping procedure to reduce the number of equations, such as that proposed in [20]. Such expensive calculations are unnecessary when the nucleation process of clusters has not been well studied. Here, we use the mean-size approximation, where the mean values of $r^{j}_{\mathrm{v,i}}$ for the sessile vacancy and interstitial loops are found via the relationship between the loop number density, N, the total number of defects in the loops of any particular type, S, and the loop Burgers vector $\mathbf{b}$:

$$S = \pi r^2 b N. \tag{16}$$

The values N and S are found from 'exact' equations, which do not require knowledge of the size-distribution function. The total numbers of defects (per atomic site) in the loops change with time according to the following equations.

$$\dot{S}^m_{\mathrm{v}} = 2\pi r^m_{\mathrm{v}} N^m_{\mathrm{v}} \left(D_{\mathrm{v}} C_{\mathrm{v}} - D_{\mathrm{i}} C_{\mathrm{i}} \right) - k^2_{\mathrm{v}m} n^{\mathrm{g}}_{\mathrm{i}} D_{\mathrm{cl}} C^m_{\mathrm{cl}}, \tag{17}$$

$$\dot{S}^m_{\mathrm{i}} = -2\pi r^m_{\mathrm{i}} N^m_{\mathrm{i}} \left(D_{\mathrm{v}} C_{\mathrm{v}} - D_{\mathrm{i}} C_{\mathrm{i}} \right) + k^2_{\mathrm{i}m} n^{\mathrm{g}}_{\mathrm{i}} D_{\mathrm{cl}} C^m_{\mathrm{cl}}, \tag{18}$$

$$\dot{S}^{\mathrm{c}}_{\mathrm{v}} = 2\pi r^{\mathrm{c}}_{\mathrm{v}} N^{\mathrm{c}}_{\mathrm{v}} \left(D_{\mathrm{v}} C_{\mathrm{v}} - D_{\mathrm{i}} C_{\mathrm{i}} \right), \tag{19}$$

where the total sink strengths of sessile dislocation loops for glissile SIA clusters are given by

$$k^2_{\mathrm{v}m} = 2\pi^2 r_{\mathrm{cvl}} r^m_{\mathrm{v}} N^m_{\mathrm{v}} \left(\frac{\pi r_{\mathrm{cd}}}{2} \rho^m_{\mathrm{d}} + \pi^2 r_{\mathrm{cvl}} r^m_{\mathrm{v}} N^m_{\mathrm{v}} + \pi^2 r_{\mathrm{cil}} r^m_{\mathrm{i}} N^m_{\mathrm{i}} \right), \tag{20}$$

$$k^2_{\mathrm{i}m} = 2\pi^2 r_{\mathrm{cil}} r^m_{\mathrm{i}} N^m_{\mathrm{i}} \left(\frac{\pi r_{\mathrm{cd}}}{2} \rho^m_{\mathrm{d}} + \pi^2 r_{\mathrm{cvl}} r^m_{\mathrm{v}} N^m_{\mathrm{v}} + \pi^2 r_{\mathrm{cil}} r^m_{\mathrm{i}} N^m_{\mathrm{i}} \right), \tag{21}$$

where r_{cvl} and r_{cil} are the capture radii of sessile vacancy and interstitial prismatic loops for SIA clusters. These equations are just generalized versions of Eq. (4) ([11] and [16]).

It follows from Eq. (16)-(19) that the mean radii of the loops change with irradiation dose according to the following equations

$$k_{vm}^2 = 2\pi^2 r_{\mathrm{cvl}} r_{\mathrm{v}}^m N_{\mathrm{v}}^m \left(\frac{\pi r_{\mathrm{cd}}}{2} \rho_{\mathrm{d}}^m + \pi^2 r_{\mathrm{cvl}} r_{\mathrm{v}}^m N_{\mathrm{v}}^m + \pi^2 r_{\mathrm{cil}} r_{\mathrm{i}}^m N_{\mathrm{i}}^m \right), \tag{22}$$

$$\frac{dr_{\mathrm{v}}^m}{d\phi} = (1-\varepsilon_{\mathrm{r}})\varepsilon_{\mathrm{i}}^{\mathrm{g}} \frac{1}{\rho} \left(1 - \frac{k_{vm}^2}{2\pi r_{\mathrm{v}}^m N_{\mathrm{v}}^m} \frac{\rho}{3k_m^2} \right), \tag{23}$$

$$\dot{S}_{\mathrm{i}}^m = -2\pi r_{\mathrm{i}}^m N_{\mathrm{i}}^m \left(D_{\mathrm{v}} C_{\mathrm{v}} - D_{\mathrm{i}} C_{\mathrm{i}} \right) + k_{im}^2 n_{\mathrm{i}}^{\mathrm{g}} D_{\mathrm{cl}} C_{\mathrm{cl}}^m, \tag{24}$$

$$\dot{S}_{\mathrm{v}}^{\mathrm{c}} = 2\pi r_{\mathrm{v}}^{\mathrm{c}} N_{\mathrm{v}}^{\mathrm{c}} \left(D_{\mathrm{v}} C_{\mathrm{v}} - D_{\mathrm{i}} C_{\mathrm{i}} \right), \tag{25}$$

2.6. Growth strains

To formulate equations for the strain rates, let us first consider the change of the quantities E: the net numbers of SIAs (i.e. the number of SIAs minus number of vacancies) accumulated by dislocations and loops in different directions. It follows from Eqs. (1)-(3) that these are equal to the sums of the contributions from glissile SIA clusters (for prismatic directions), and PDs captured by dislocations and sessile loops (for all directions) ($m = \mathbf{a_1}, \mathbf{a_2}, \mathbf{a_3}$):

$$\dot{E}_m = \frac{1}{3}\chi G - \rho_m \left(D_{\mathrm{v}} C_{\mathrm{v}} - D_{\mathrm{i}} C_{\mathrm{i}} \right), \tag{26}$$

$$\dot{E}_{\mathrm{c}} = -\rho_{\mathrm{c}} \left(D_{\mathrm{v}} C_{\mathrm{v}} - D_{\mathrm{i}} C_{\mathrm{i}} \right), \tag{27}$$

In these equations, the SIA cluster contribution to strains is accounted for by the first term on the RHS of Eq. (26), while the other terms are due to collisions of dislocations and sessile loops with the point defects. The fraction of SIAs produced by irradiation going to sessile loops nuclei is assumed to be negligibly small as compared to that forming glissile clusters, and the corresponding terms are ignored. With these equations, the strains along the principle axes of the Cartesian coordinate system introduced in Section 2.3 assume the following form (cf. Eqs. (10)-(12); see Appendix for the strain in arbitrary direction):

$$\varepsilon_{\mathrm{x}} = E_{\mathrm{a}_1} + \left(E_{\mathrm{a}_2} + E_{\mathrm{a}_3} \right) \cos^2 \left(\pi / 3 \right), \tag{28}$$

$$\varepsilon_{\mathrm{y}} = \left(E_{\mathrm{a}_2} + E_{\mathrm{a}_3} \right) \sin^2 \left(\pi / 3 \right), \tag{29}$$

$$\varepsilon_z = E_{\mathrm{c}}. \tag{30}$$

2.7. Dislocation velocities

Finally, we note that the dislocation climb velocities V_j are in general different for different directions and can be calculated from the following relationship

$$\dot{E}_j = \rho_j V_j b_j. \tag{31}$$

These can be used for calculating creep rates in the framework of the 'climb-induced glide' model [21]. Thus, our RG model provides a link to the description of creep.

3. Calculations

Fig. 1 shows the evolution of the number densities of interstitial-type prismatic loops and vacancy-type basal loops, calculated using Eqs. **Error! Reference source not found.** and **Error! Reference source not found.** with the parameters collected in Table 1. (The total number density of prismatic loops is defined as the sum $N^{\mathrm{a,max}} = N^{\mathrm{a1,max}} + N^{\mathrm{a2,max}} + N^{\mathrm{a3,max}}$.) These functions are close to experimental data in [22] and are used as the basic parameter set for the calculations presented below.

A computer code RIMD-ZR.V1 (Radiation Induced Microstructure and Deformation of Zr, Version 1) implementing the scheme described above has been developed and used to study evolution of the microstructure during neutron irradiation. Selected results are presented below.

3.1. Fitting of the model to experimental data

Fig. 2 shows the results of using experimental data from [22] to adjust model parameters. The NRT standard dose was calculated from the fluence, assuming that 10^{25} n/m^2=1 dpa. The number densities of dislocation loops shown in Fig. 1 were used. The best fit parameters were: ε_{r} =0.9 and $\varepsilon_{\mathrm{i}}^{\mathrm{g}}$ =0.2; while the interaction radii of the SIA clusters with dislocations and loops were taken to be $r_{\mathrm{cd}} = r_{\mathrm{cvl}} = r_{\mathrm{cil}}$ = 0.6 nm. The value of χ= 0.02 was found to be the same as that extracted from experiments on fcc Cu in [13]. These parameters were used as the basic set (see Table 1) in the following calculations.

The results in Fig. 2 were obtained for an isotropic distribution of prismatic dislocations. The *c* strain in this case is two times larger than that along any of the *a* directions. This is not always the case in experiments, as shown in Fig. 3a [22], where the *c* strain is even smaller than *a* strain. One of the reasons for this observation may be a non-isotropic distribution of prismatic dislocations. The latter effect is considered in the following sections.

The strain behavior calculated for a wider dose range, which includes the break-away stage, is presented in Fig. 3 for the same parameters as in Fig. 2. These results demonstrate that the function chosen to describe nucleation of *c*-type vacancy loops gives strain values during the break-away stage which are similar to those observed experimentally in [22].

The observed values of ~10 nm for the radii of *a*-type interstitial loops and ~300 nm for the vacancy *c* loops are also reproduced well by this parameter set, as shown in Fig. 4.

Note that a small decrease in the mean size of *a* loops in the intermediated dose range may be an artificial effect due to the mean-size approximation used. However, this is not a problem since the more important integral values, which affect strain behavior, behave well; e.g. the loop sink strength increases steadily with increasing irradiation dose, as shown in Fig. 5.

3.2. Effect of cold work

The effect of cold-work on the strain behavior is demonstrated in Fig. 6. As can be seen from the figure, an increase of all dislocation densities in the basic parameter set (Table 1) by an order of magnitude increases the strains (dashed line, cf. with solid line calculated with the basic parameter set), but the tendency toward strain saturation is yet maintained. Another tenfold (or higher) increase of the densities gives steep straight (dotted) line with the slope ~1.7×10^{-3} dpa^{-1}, as indicated in the figure. This is in a good agreement with the maximum of ~10^{-3} dpa^{-1} observed for swaged Zr [22]. The value of ~10^{-3} dpa^{-1} is reproduced by our calculations, when the ratio of *a* to *c* dislocation densities is two times higher: $\rho_{\mathrm{d}}^{\mathrm{a}} / \rho_{\mathrm{d}}^{\mathrm{c}} = 10$ (dash-dotted line, the ratio of dislocation densities in indicated in the figure).

3.3. Radiation growth at high doses

Fig. 7 shows the dose dependence of growth strain at high irradiation doses of up to 100 dpa. Two calculations, for low and high dislocation densities, are presented. These show remarkable qualitative, as well as quantitative, differences in the strain behavior in the dose range up to 2.5 dpa in Fig. 6 (cf. solid and dotted lines). The difference between the predicted strains diminishes at high doses. This is because the sink strength of sessile loops becomes significantly higher than that of pre-existing dislocations very early during irradiation due to nucleation and growth of sessile loops. This is demonstrated in Figs. 8 and 9, which show the dose dependence of the loop radii and the loop sink strength, respectively. The sink strength of these loops then governs the strain behavior, which is independent of initial dislocation density. In the high-dose range, the calculations presented in Fig. 7 depend mainly on the ratio of number densities of sessile *a*-type interstitial and *c*-type vacancy loops, $N_{\mathrm{i}}^{\mathrm{a,max}} / N_{\mathrm{v}}^{\mathrm{c,max}}$. A value of 10 was used in these calculations, as indicated in the figure.

Fig. 10 shows the decrease of growth strain with increasing ratio of *a*- to *c*-loop densities. By suppressing the nucleation of *c*-type loops, one can decrease the strains and thereby enhance the radiation resistance of Zr.

Thus, at relatively high irradiation doses, the dislocation loops govern the strain behavior. In this case, one can derive an equation for the strain rate as follows. In the case considered, the number of vacancies in the *c*–type vacancy loops is approximately equal to the number of SIAs in *a*–type interstitial loops: $\pi\left(r_{\mathrm{i}}^{\mathrm{a}}\right)^2 N_{\mathrm{i}}^{\mathrm{a,max}} b = \pi\left(r_{\mathrm{v}}^{\mathrm{c}}\right)^2 N_{\mathrm{v}}^{\mathrm{c,max}} b$, and it can be obtained from Eqs. (8), (9) and (13) that

$$\frac{d\varepsilon_z}{d\phi} = -2\frac{d\varepsilon_x}{d\phi} = -2\frac{d\varepsilon_y}{d\phi} = -\chi\frac{1}{1+\sqrt{N_i^{a,max}/N_v^{c,max}}}. \tag{32}$$

According to this equation, if the number density of *c*-type vacancy loops is low as compared to interstitial prismatic loops: $N_i^{a,max} >> N_v^{c,max}$, the strain rate is proportional to the square root of the ratio of the loop number densities:

$$\left(\frac{d\varepsilon_z}{d\phi}\right)_{\phi\to\infty} \approx -\chi\sqrt{\frac{N_v^{c,max}}{N_i^{a,max}}}. \tag{33}$$

Note that since the nucleation period is limited, the asymptotic values of the strain rates can be predicted at relatively low doses, when the loop number densities reach steady state.

3.4. Effect of vacancy loops on radiation growth

It can readily be shown using Eqs. (17)-(18) and (5)-(7) that, if the total dislocation density in one direction (e.g. $\mathbf{a}_1$) is higher than in the other two directions, then the vacancy loops grow in this direction, while interstitial loops grow in the other two directions. If the dislocation densities in $\mathbf{a}_2$ and $\mathbf{a}_3$ directions are equal, the evolution of the dislocation densities in $\mathbf{a}_1$, $\mathbf{a}_2$ and $\mathbf{a}_3$ directions are described by the following equations:

$$\frac{d\rho_{a_1}}{d\phi} = \chi\frac{2\pi N_v^{a_1}}{3b}\left[\frac{2\left(\rho_{a_1}-\rho_{a_2}\right)-\rho_c}{\rho_{a_1}\rho}\right], \tag{34}$$

$$\frac{d\rho_{a_2}}{d\phi} \equiv \frac{d\rho_{a_3}}{d\phi} = \chi\frac{2\pi N_i^{a_2}}{3b}\left[\frac{\left(\rho_{a_1}-\rho_{a_2}\right)+\rho_c}{\rho_{a_2}\rho}\right]. \tag{35}$$

The vacancy loops can grow, when the RHS of Eq. (34) is positive, meaning that

$$2\left(\rho_{a_1}-\rho_{a_2}\right) > \rho_c. \tag{36}$$

This may be true in the beginning of irradiation, when only preexisting dislocations are present. However, if interstitial *a*-loop line density accumulates faster than that of *a* vacancy loops, the RHS of Eq. (31) may become negative, and the vacancy loops will start to dissolve. The line density of interstitial loops increases faster if the ratio of Eqs. (34) and (35) is smaller than unity:

$$\frac{\dot{\rho}_{a_1}}{\dot{\rho}_{a_2}} = \frac{2N_v^{a_1}\rho_{a_2}}{N_i^{a_2}\rho_{a_1}}\left[1-\frac{3}{2}\frac{\rho_c}{\left(\rho_{a_1}-\rho_{a_2}\right)+\rho_c}\right] < 1. \tag{37}$$

This scenario is demonstrated in Figs. 11 and 12, which were calculated with $N_{\mathrm{v}}^{\mathrm{a}_1} = N_{\mathrm{i}}^{\mathrm{a}_2}$ and $\rho_{\mathrm{d}}^{\mathrm{a}_1} = 6\rho_{\mathrm{d}}^{\mathrm{a}_2}$ (see inset in Fig. 12). As can be seen, the vacancy loops in the $\mathbf{a}_1$ direction and interstitial loops in $\mathbf{a}_2$ and $\mathbf{a}_3$ directions grow very fast for a short period. Then, vacancy loops start to dissolve, and interstitial loops start to grow in the $\mathbf{a}_1$ direction. Vacancy loops in the $\mathbf{a}_2$ and $\mathbf{a}_3$ directions grow temporarily then shrink during a transition period, when vacancy loops shrink in the $\mathbf{a}_1$ direction. Then, interstitial-type loops grow in all three *a* directions.

Fig. 12 shows that, in the case considered, the strain along the direction where vacancy loops grow is negative for about six dpa. Then, after vacancy loops dissolved, the strain becomes positive and increases similarly to those in other two directions. This picture is similar to that observed experimentally in [22]. At higher irradiation doses the *x* and *y* strains approach each other, as shown in the black dotted and dashed lines in Fig. 13.

Fig. 13 shows the dose dependence of the growth strain for the same case as in Fig. 12, designated as low dislocation density, and for the case when all dislocation densities are increased by an order of magnitude, designated as high dislocation density. The corresponding changes of the loop radii are shown in Fig. 14. For the higher dislocation density, vacancy loops grow over a longer dose range, but the accumulation of loops eventually breaks the inequality of Eq. (36). Then, the *x* strain changes its sign and approaches the asymptotic behavior of the *y* strain. Thus, the observed negative *a* strains, which have been discussed extensively in the literature (see, e.g. [17]), are explained by the present calculations. Moreover, it is shown that the negative strains are expected to exist only in a certain dose range and disappear at high enough doses.

In the calculations discussed above, vacancy loops grow in one *a* direction and interstitial loops in the other two *a* directions, which is due to corresponding distribution of initial dislocation densities in these direction. The situation is symmetric; vacancy loops may grow in two directions and interstitial loops in one direction if the dislocation densities in two *a* directions are higher. This is demonstrated in Figs. 15 and 16 for the loop strains and radii, respectively. The description of the figures is the same as for Figs. 13 and 14, and the scenario in which vacancy loops initially grow but then dissolve is realized in this case as well.

3.5. The maximum strain rate

In the previous section, the assumption that $N_{\mathrm{v}}^{\mathrm{a}_1} = N_{\mathrm{i}}^{\mathrm{a}_2}$ was used and vacancy loops eventually dissolve in all the cases considered. This is because interstitial loops grow faster than vacancy loops, i.e. their density increases more rapidly, and, as a consequence, the condition of Eq. (36) is eventually broken. The maximum strain rate is then limited by Eq. (32). This equation gives the maximum *a*-strain rate of ~0.16% dpa^{-1}, which is an order of magnitude smaller than the maximum value possible in the proposed model, which is about 1% dpa^{-1} for $\chi = 0.02$.

To obtain high strain rates, which are close to the theoretical maximum of our model, i.e. ~1% dpa^{-1}, one should assume that vacancy loops nucleate faster than interstitial loops, so that vacancy loop density increases faster, i.e. $\dot{\rho}_{\mathrm{a}_1} / \dot{\rho}_{\mathrm{a}_2} \approx 2N_{\mathrm{v}}^{\mathrm{a}_1}\rho_{\mathrm{a}_2} / N_{\mathrm{i}}^{\mathrm{a}_2}\rho_{\mathrm{a}_1} > 1$. Fig. 17 shows the

strain behavior for different maximum densities of *a*-type vacancy loops in one of the *a* directions. The black solid line shows the basic case, which is same as in Fig. 7, for which *x* and *y* strains are both positive at high irradiation doses and the maximum strain reached at 100 dpa is ~16%. For 10 and 100 times higher maximum values of the vacancy loop number density, the *x* ($\mathbf{a}_1$ direction) strain remains always negative, the *z* strain close to zero, and the *y* strain positive and close to the absolute value of the *x* strain. For the highest number density, the *y* strain reaches ~80% and the *x* strain reaches the same negative value, which is close to theoretical maximum. Thus, maximum *a*-strain rates of the order of 1% dpa^{-1} may realize if one *a* direction expands due to accumulation of *a*-type interstitial loops and the other contracts due to *a*-type vacancy loops, with relatively small changes in *c* direction.

3.6. Dislocation climb velocities

Figs. 19 and 20 show dose dependences of dislocation climb velocities. As can be seen, *c* dislocations climb faster than *a* dislocations because of their relatively lower density. They climb only by capturing an excess of vacancies and the climb rate decreases steadily because of constant increase of the total sink strength for vacancies due to growth of dislocation loops.

In contrast, *a* dislocations climb slower than *c* dislocations due to their higher density, and the dose dependence of their climb rate is more complicated. They capture both PDs and SIA clusters, and their climb rate increases at doses ~3-6 dpa due to nucleation and growth of vacancy *c* loops, which capture vacancies. At higher doses, the velocity starts decreasing again, as seen on Fig. 19.

4. Summary

1. The computer code RIMD-ZR.V1 (Radiation Induced Microstructure and Deformation of Zr, Version 1), which implements the model of radiation growth of Zr proposed recently in [1] and [2], and uses the mean-size approximation for the description of sessile vacancy and interstitial loops, has been developed.
2. The basic parameters of the model (Table 1) have been fitted to the experimental data available. The main parameters defining primary damage produced by displacement cascade: ε_r=0.9, ε_i^g =0.2, are the same as those extracted from swelling experiments on fcc copper in [13], and those required to reproduce steady-state swelling rates observed in austenitic stainless steels at high irradiation doses (see estimates in [14]).
3. The calculations reproduce the observed growth stages, including the 'break-away' growth of pre-annealed materials, the negative strains in prismatic directions and co-existence of vacancy- and interstitial-type prismatic loops.
4. The strain rates at high enough doses are determined by the ratio of number densities of interstitial prismatic and vacancy basal loops, see Eq. (32). These may, thus, be predicted at relatively small doses, when the nucleation stage is completed.
5. The calculations confirm the maximum strain rate of ~1% dpa^{-1} predicted by the model [1] and [2]. This may occur for highly anisotropic distribution of prismatic dislocations. It

requires that the vacancy and interstitial prismatic loops coexist, so that the crystal expands in one *a* direction and contracts in the other, with very small *c* strain.

6. The computer code provides the climb velocities for dislocations of different Burgers vector orientation, which are required for calculating creep rates using the climb-induced glide model. Thus, the model provides a necessary link to the description of creep.

The calculations have revealed a crucial dependence of the strains on the loop number densities, especially in the high dose limit, see Eq. (33). Hence, further progress in this area is only possible if the physical mechanisms of sessile loop nucleation are elucidated.

Finally, we would like to emphasize that the predicted maximum value of the RG strain rate for Zr of ~1% dpa^{-1} is the same as the maximum swelling rate found in cubic materials (see discussion in [14]). This follows from similarity of cascade-induced radiation damage in the bcc, fcc and hcp metallic crystals, and indicates that the Production Bias Model [16], which was originally developed for cubic materials, provides a general framework for the theory of radiation damage.

Acknowledgements

This research was supported by the Consortium for Advanced Simulation of Light Water Reactors (http://www.casl.gov), an Energy Innovation Hub (http://www.energy.gov/hubs) for Modeling and Simulation of Nuclear Reactors under U.S. Department of Energy Contract No. DE-AC05-00OR22725.

Appendix

Generally, the strains in prismatic directions is described by a two-dimensional tensor, ε_{ik}, which can be found using Eq. (26). In a Cartesian coordinate system with the x axis lying in the basal plane and making angle α with $\mathbf{a}_1$ direction (see Fig. 20):

$$\varepsilon_{\mathrm{x}} = E_{\mathrm{a}_1}\cos^2\alpha + E_{\mathrm{a}_2}\cos^2\left(\alpha-\pi/3\right) + E_{\mathrm{a}_3}\cos^2\left(\alpha+\pi/3\right). \tag{38}$$

$$\varepsilon_{\mathrm{y}} = E_{\mathrm{a}_1}\sin^2\alpha + E_{\mathrm{a}_2}\sin^2\left(\alpha-\pi/3\right) + E_{\mathrm{a}_3}\sin^2\left(\alpha+\pi/3\right). \tag{39}$$

It can readily be shown that ε_{ik} is diagonal when x and y axes make α_0 and $\pi/2$-α_0 angles with $\mathbf{a}_1$, respectively, and z is along $\mathbf{c}$, where

$$\alpha_0 = \frac{1}{2}arctg\left[\frac{\sqrt{3}\left(E_{\mathrm{a}_2}-E_{\mathrm{a}_3}\right)}{2E_{\mathrm{a}_1}-E_{\mathrm{a}_2}-E_{\mathrm{a}_3}}\right] \pm \frac{\pi}{2}k, \tag{40}$$

and k is an integer. Eq. (40) is derived from Eq. (38) by equating $d\varepsilon_{\mathrm{x}}/d\alpha$ to zero. In such a system, the strain field is described by an ellipsoid with x and y being the principal axes [23], while the strain along any particular direction $\mathbf{l}$ is given by a simple sum:

$$\varepsilon_{\mathbf{l}} = \varepsilon_{\mathrm{x}}\cos^2\left(\mathbf{l},x\right) + \varepsilon_{\mathrm{y}}\cos^2\left(\mathbf{l},y\right) + \varepsilon_{\mathrm{z}}\cos^2\left(\mathbf{l},z\right), \tag{41}$$

where $\left(\mathbf{l},x\right)$ denotes the angle between the two directions in the brackets. In other coordinate systems, i.e. when $\alpha \neq \alpha_0$, the difference in the quantities defined by Eqs. (41) and (38) is given by $\frac{\sqrt{3}}{4}\left(\varepsilon_{\mathrm{a}_3}-\varepsilon_{\mathrm{a}_2}\right)\sin(2\alpha)$. Hence, the strains along principal axes of the coordinate system with the x axis along $\mathbf{a}_1$ direction, i.e. for $\alpha_0 = 0$, are always correct.

As we argue in Sections 3.3 and 3.4, at relatively high doses the dislocation structure tends to be isotropic in prismatic directions, hence one can assume that $\alpha_0 = 0$. At low doses and anisotropic distribution of prismatic dislocations, such an assumption is, strictly speaking, incorrect, and the exact Eq. (38) should be used.

References

[1] S.I. Golubov, A.V. Barashev, R.E. Stoller, ORNL Report: ORNL/TM-2011/473, (2011), 21 p.

[2] S.I. Golubov, A.V. Barashev, R.E. Stoller, ASTM conference proceedings of 17th International Symposium on Zirconium in the Nuclear Industry, Hyderabad, India, (in preparation).

[3] S.N. Buckley, Properties of Reactor Materials and Effects of Radiation Damage, ed. W.J. Littler (Butterworths, London, 1962), p. 413.

[4] R.A. Holt, J. Nucl. Mater., 372 (2008), pp. 182-214.

[5] C.H. Woo, U.M. Gösele, J. Nucl. Mater., 119 (1983), pp. 219-228.

[6] C.H. Woo, J. Nucl. Mater., 159 (1988), pp. 237-256.

[7] B. von Guerard, J. Peisl, J. Appl. Cryst., 8 (1975), p. 161.

[8] S.J. Wooding, L.M. Howe, F. Gao, A.F. Calder, D.J. Bacon, J. Nucl. Mater., 254 (1998), pp. 191-204.

[9] R.E. Stoller, "Primary Radiation Damage Formation," in Comprehensive Nuclear Materials, R. J. M. Konings, T. R. Allen, R. E. Stoller, and S. Yamanaka, Editors, Elsevier Ltd., Amsterdam, 2012, pp. 293-332.

[10] N. De Diego, Y.N. Osetsky, D.J. Bacon, In: Proceedings of MRS Fall Meeting; Boston, MA, USA; (2000), p. 200.

[11] A.V. Barashev, S.I. Golubov, H. Trinkaus, Phil. Mag. A, 81 (10) (2001), pp. 2515-2532.

[12] R.A. Holt, C .H. Woo, C.K. Chow, J. Nucl. Mater., 205 (1993), pp. 293-300.

[13] S.I. Golubov, B.N. Singh, H. Trinkaus, Phil. Mag. A, 81 (10) (2001), pp. 2533-2552.

[14] A.V. Barashev, S.I. Golubov, Phil. Mag., 89 (31) (2009), pp. 2833-2860.

[15] B.N. Singh, S.I. Golubov, H. Trinkaus, A. Serra, Yu.N. Osetsky, A.V. Barashev, J. Nucl. Mater., 251 (1997), pp. 107-122.

[16] S.I. Golubov, A.V. Barashev, R.E. Stoller, "Mean Field Reaction Rate Theory", In: Encyclopedia of Comprehensive Nuclear Materials, Chapter 29, edited by Rudy Konings, Elsevier Ltd. (2011), pp. 357-391.

[17] M. Griffiths, R.A. Holt, A. Rogerson, J. Nucl. Mater., 225 (1995), pp. 245-258.

[18] R. Risbet, V. Levy, J. Nucl. Mater., 50 (1974), pp. 116-118.

[19] Y. de Carlan, C. Regnard, M. Griffiths, D. Gilbon, C. Lemaignan, ASTM STP 1295 (1996), p. 638.

[20] S.I. Golubov, A.M. Ovcharenko, A.V. Barashev, B.N. Singh, Phil. Mag. A, 81 (3) (2001), pp. 643-658.

[21] G.J.C. Carpenter, R.H. Zee, A. Rogerson, J.F. Watters, J. Nucl. Mater., 159 (1988), pp. 86-100.

[22] Gittus

[23] L.D. Landau, E.M. Lifshitz, Theory of Elasticity, 3rd Edition, (Course of theoretical physics, vol. 7), Elsevier, 1986, p. ???.

Figure captions

Fig. 1. Dependence of vacancy and interstitial loop number densities on the irradiation dose.
Fig. 2. Comparison of the calculated growth strain with experimental measurements (Fig. 3b in [22]), closed symbols for iodide and open symbols for zone-refined purity.
Fig. 3. Growth strain for the same basic set of parameters (Table 1) as in Fig. 2, but for a wider dose range. Note that the strain values during the break-away stage are similar to those observed experimentally.
Fig. 4. Calculated dose dependence of the sessile loop radii, which reproduce well the experimental values.
Fig. 5. Calculated dose dependence of the sessile loop sink strength.
Fig. 6. Effect of cold work on the growth strain behavior. Solid line is calculated with the basic parameter set (Table 1). Dashed line is calculated with all dislocation densities in the basic parameter set increased by an order of magnitude. Dotted line is calculated with the hindred times higher dislocation densities. Dash-dotted line is calculated with $\rho_{\mathrm{d}}^{\mathrm{a}} / \rho_{\mathrm{d}}^{\mathrm{c}} = 10$, i.e. two times higher ratio of *a* to *c* dislocation densities.
Fig. 7. Dose dependence of growth strain behavior up to hundred dpa, for high (dotted line) and low (solid line) densities of prismatic dislocations. Note that, at high doses, the strain behavior is independent of the initial dislocation density.
Fig. 8. Dose dependence of loop radii calculated for $\rho_{\mathrm{d}}^{\mathrm{a}} = 3\mathrm{x}10^{12}\,\mathrm{m}^{-2}$.
Fig. 9. Dose dependence of the loop sink strengths for $\rho_{\mathrm{d}}^{\mathrm{a}} = 3\mathrm{x}10^{12}\,\mathrm{m}^{-2}$. Note that, at high irradiation doses, the loop sink strength is much higher than the dislocation density.
Fig. 10. Decrease of growth strain with increasing ratio of *a*- to *c*-loop densities. Note an enhanced radiation resistance of Zr due to suppression of c-type loop nucleation.
Fig. 11. Dose dependence of sessile interstitial and vacancy loop radii calculated for the case in which the initial density of $\mathbf{a}_1$ dislocations is six times higher than in the other two directions. Note co-existence of vacancy- and interstitial-type prismatic loops for a limited, several dpa, period of irradiation.
Fig. 12. Same as in Fig. 11 but for growth strain. Note that the strain along the direction where vacancy loops grow and, then, positive, when vacancy loops dissolved.
Fig. 13. Dose dependence of growth strain for the same case as in Fig. 12 (designated as low dislocation density, black lines), and for the case in which all dislocation densities are increased by an order of magnitude (designated as high dislocation density, blue lines).
Fig. 14. Same as in Fig. 13 designated as high dislocation density but for the loop radii.
Fig. 15. Dose dependence of growth strain for the case when the initial density of $\mathbf{a}_1$ dislocations is ten time lower than in the other two *a* directions. Note that in this case vacancy loops initially grow and then dissolve in two *a* directions rather than one *a* direction, as in Figs. 13 and 14.
Fig. 16. Same as in Fig. 15 but for the loop radii.
Fig. 17. Strain behavior for different maximum densities of *a*-type vacancy loops in one of the *a* directions. The numbers 1, 10 and 100 are values of the ratio of $N_{\mathrm{v}}^{\mathrm{a}_1} / N_{\mathrm{i}}^{\mathrm{a}_2}$. Note that *c* strain in both cases is close to zero. Also, note that the maximum *a*-strain rates of the order of 1% dpa^{-1} is realized at high ratios.
Fig. 18. Dislocation climb velocities at small irradiation doses for *c* dislocations (dotted, blue – dislocation density 10^{12} m^{-2}; dash dot, wine – 10^{13}; dash, blue – 10^{14}) and *a* dislocations (dot dash dot, black – 10^{12}; dash dot dot, wine – 10^{13}; solid, black – 10^{14}).

Fig. 19. Dislocation velocities as in Fig. 18 but for a wider dose range.
Fig. 20. Cartesian (x, y) coordinate system on the basal plane, where x and y axes make α and $\pi/2+\alpha$ angles with $\mathbf{a}_1$ direction.

Table 1. Basic set of calculation parameters, used in calculations unless stated otherwise.

Definition	Symbol	Value
Fraction of defects recombining in cascades	ε_{r}	0.9
Fraction of SIAs produced in glissile clusters	$\varepsilon_{\mathrm{i}}^{\mathrm{g}}$	0.2
Terminal density of *a*-type sessile loops	$N^{\mathrm{a,max}}$	10^{22} m^{-3}
Terminal dose for nucleation of sessile *a* loops	$\phi_{\mathrm{max}}^{\mathrm{a}}$	3.84 dpa
Terminal density of *c*-type sessile vacancy loops	$N^{\mathrm{c,max}}$	10^{21} m^{-3}
Starting dose for nucleation of *c* vacancy loops	ϕ_{0}^{c}	3 dpa
Terminal dose for nucleation of *c* vacancy loops	$\phi_{\mathrm{max}}^{\mathrm{c}}$	23 dpa
Nucleation parameter for *c* loops in Eq. (28)	A	5
Burgers vector of *a* loops	b_{a}	3×10^{-10} m
Burgers vector of *c* loops	b_{c}	5×10^{-10} m
Capture radii of dislocations, and sessile vacancy and interstitial prismatic loops for SIA clusters	$r_{\mathrm{cd}}, r_{\mathrm{cvl}}, r_{\mathrm{cil}}$	6×10^{-10} m
Densities of a_1, a_2, a_3 dislocations	$\rho_{\mathrm{d}}^{\mathrm{a}_1}, \rho_{\mathrm{d}}^{\mathrm{a}_2}, \rho_{\mathrm{d}}^{\mathrm{a}_3}$	10^{12} m^{-2}
Density of *c* dislocations	$\rho_{\mathrm{d}}^{\mathrm{c}}$	0.6×10^{12} m^{-2}
Neutron fluence corresponding to 1 dpa of the NRT standard dose	---	10^{25} n/m^{2}

Fig. 1.

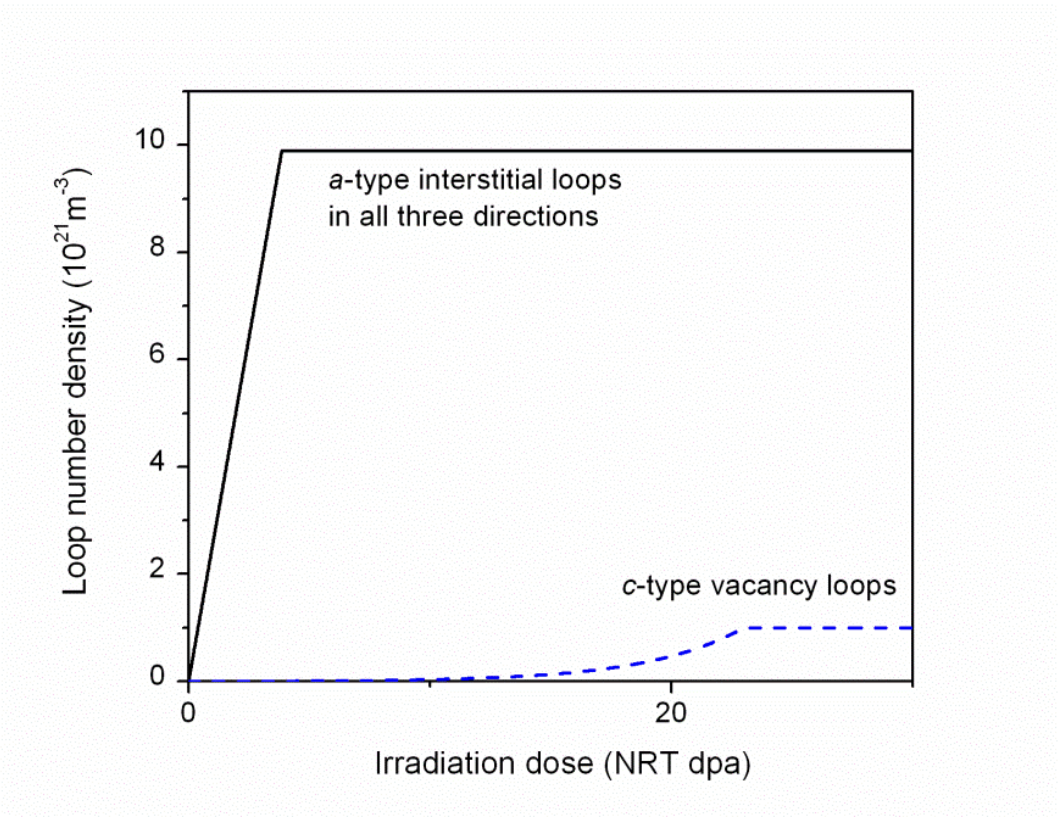
Loop number density (10^{21}m^{-3})
10
8
6
4
2
0
a-type interstitial loops
in all three directions
c-type vacancy loops
0
20
Irradiation dose (NRT dpa)

Fig. 2.

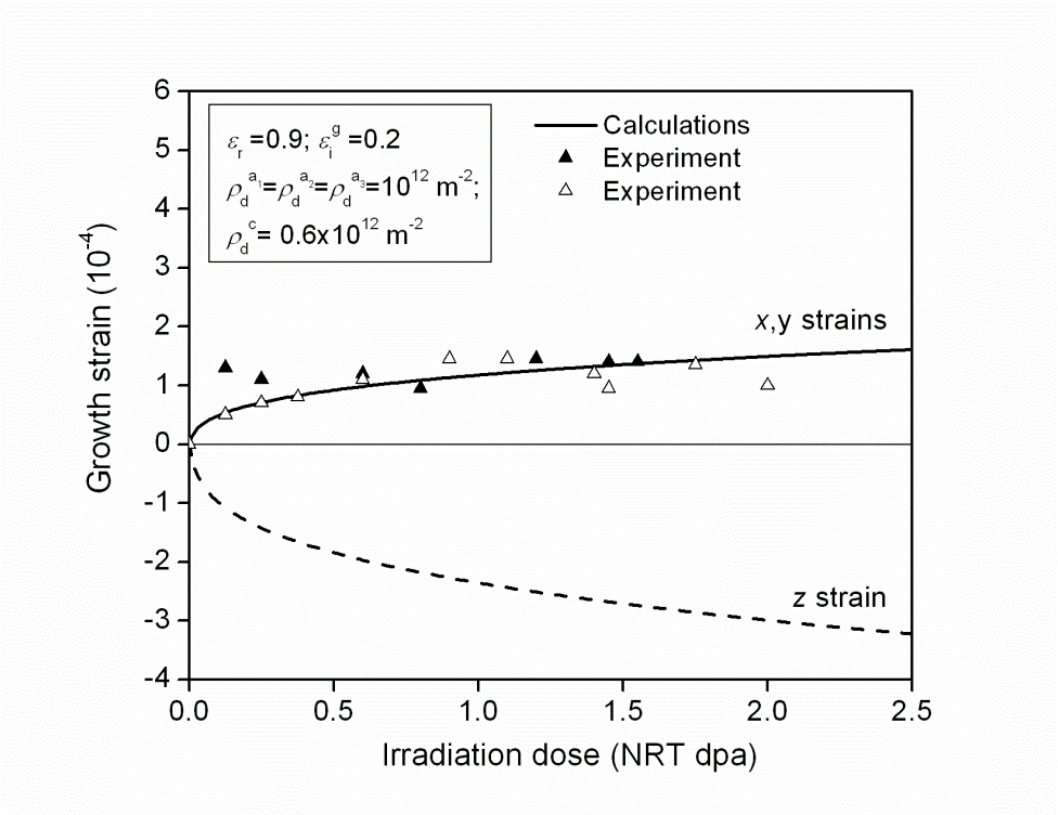
ε_r =0.9; ε_i^g =0.2
$\rho_d^{a_1}=\rho_d^{a_2}=\rho_d^{a_3}=10^{12}$ m^{-2};
ρ_d^c= 0.6x10^{12} m^{-2}
Calculations
Experiment
Experiment
x,y strains
z strain
Growth strain (10^{-4})
Irradiation dose (NRT dpa)
6
5
4
3
2
1
0
-1
-2
-3
-4
0.0
0.5
1.0
1.5
2.0
2.5

Fig. 3.

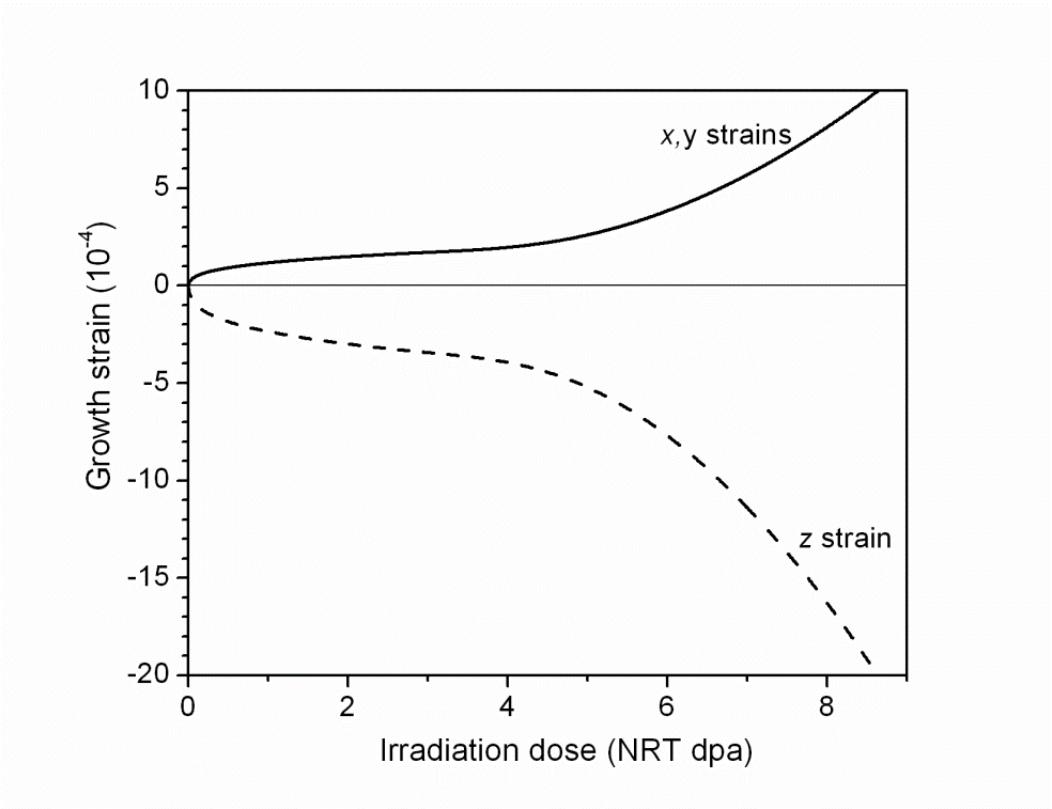
10
5
0
-5
-10
-15
-20
Growth strain (10^{-4})
0
2
4
6
8
Irradiation dose (NRT dpa)
x,y strains
z strain

Fig. 4.

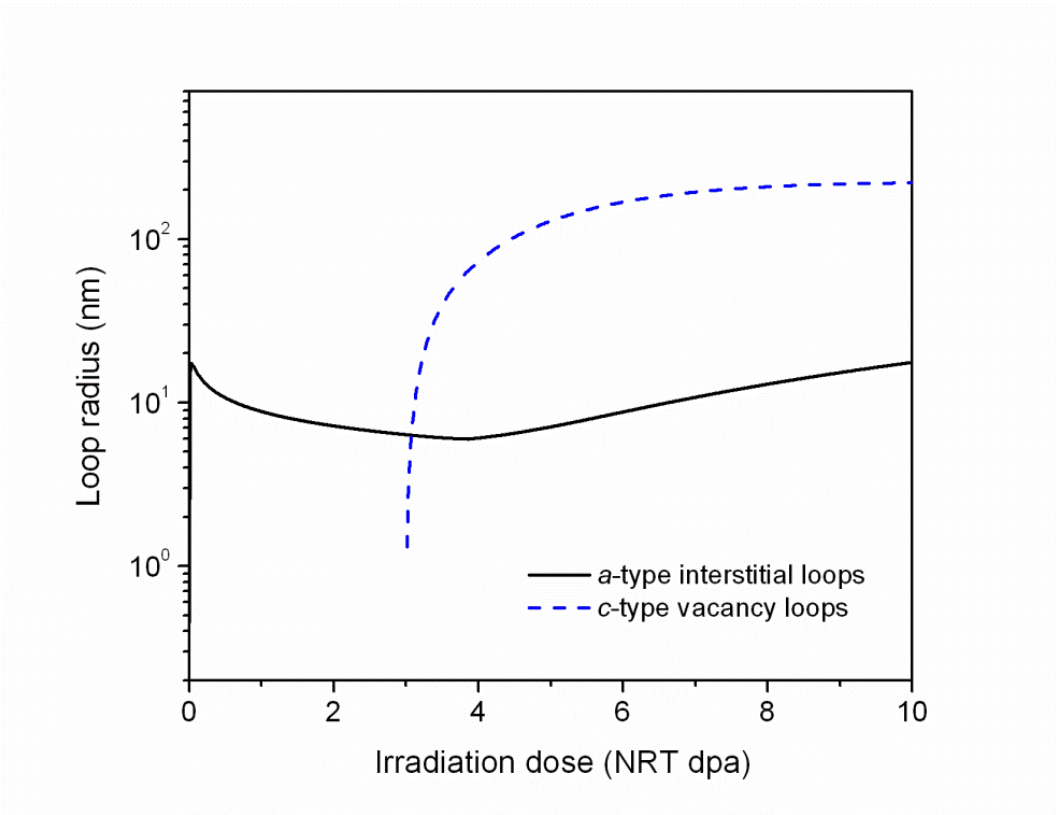
Loop radius (nm)
10^2
10^1
10^0
0
2
4
6
8
10
Irradiation dose (NRT dpa)
a-type interstitial loops
c-type vacancy loops

Fig. 5.

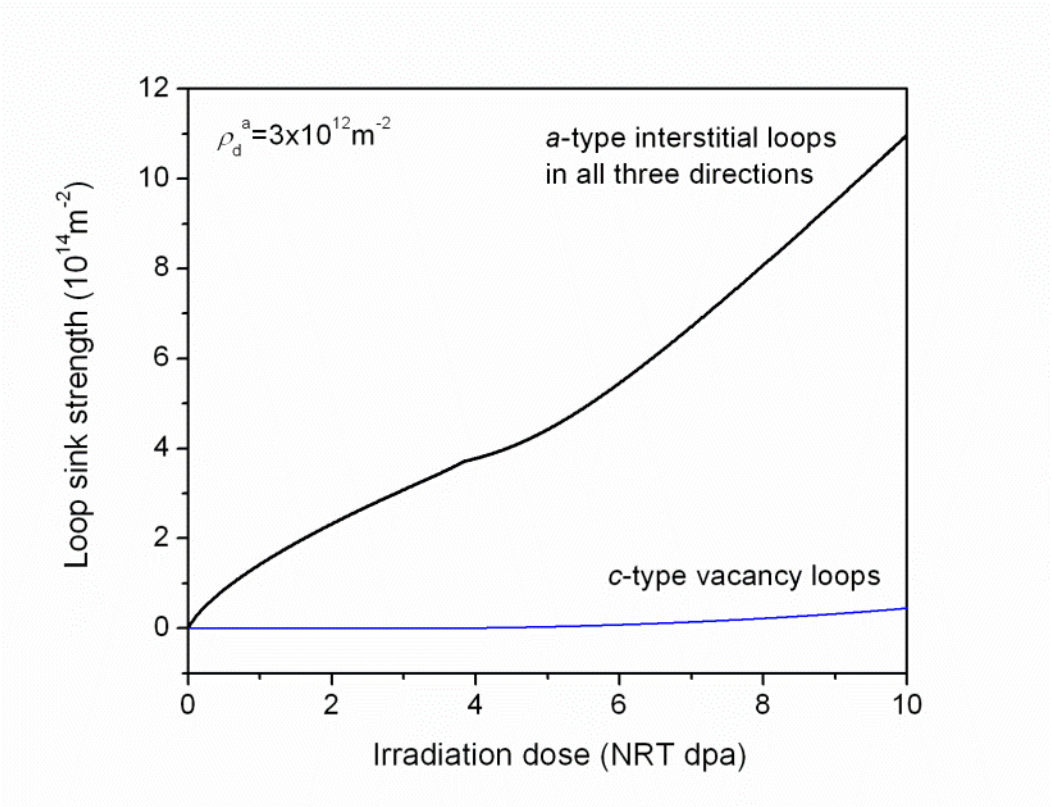
ρ_d^a=3x10^{12}m^{-2}
a-type interstitial loops
in all three directions
c-type vacancy loops
Loop sink strength (10^{14}m^{-2})
Irradiation dose (NRT dpa)
0
2
4
6
8
10
12

Fig. 6.

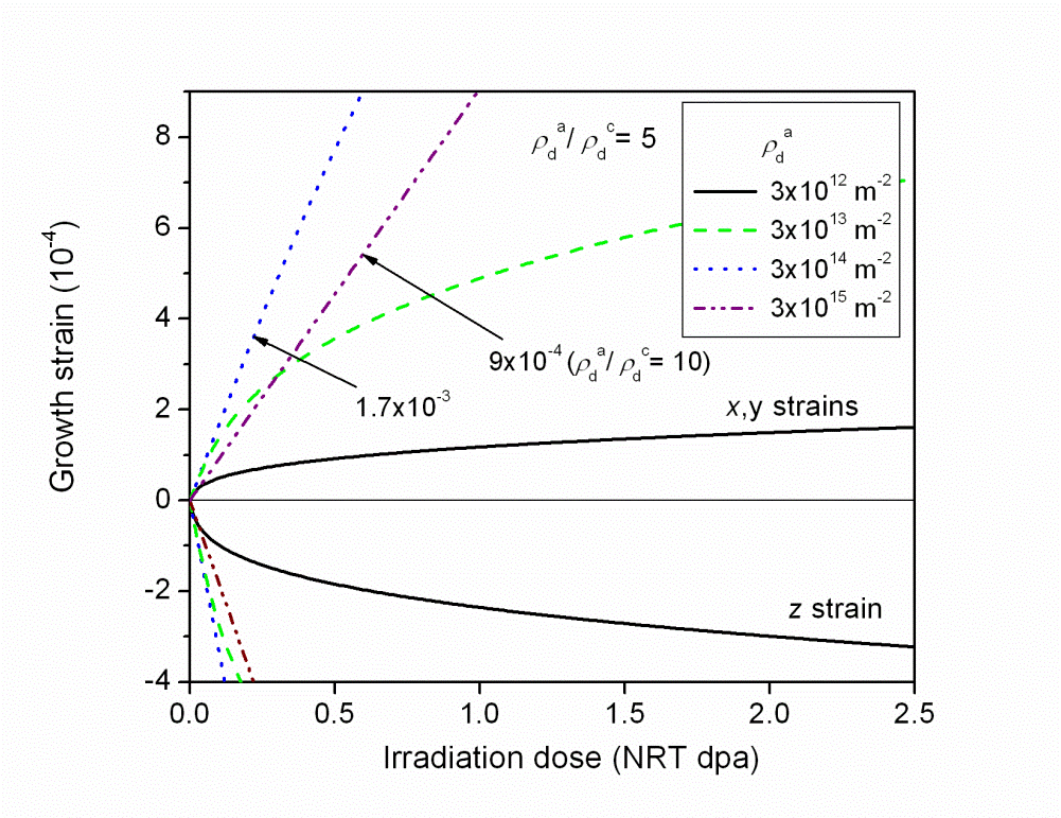
$\rho_d^a / \rho_d^c = 5$
ρ_d^a
$3x10^{12}$ m^{-2}
$3x10^{13}$ m^{-2}
$3x10^{14}$ m^{-2}
$3x10^{15}$ m^{-2}
$9x10^{-4}$ ($\rho_d^a / \rho_d^c = 10$)
$1.7x10^{-3}$
x,y strains
z strain
Growth strain (10^{-4})
Irradiation dose (NRT dpa)
8
6
4
2
0
-2
-4
0.0
0.5
1.0
1.5
2.0
2.5

Fig. 7.

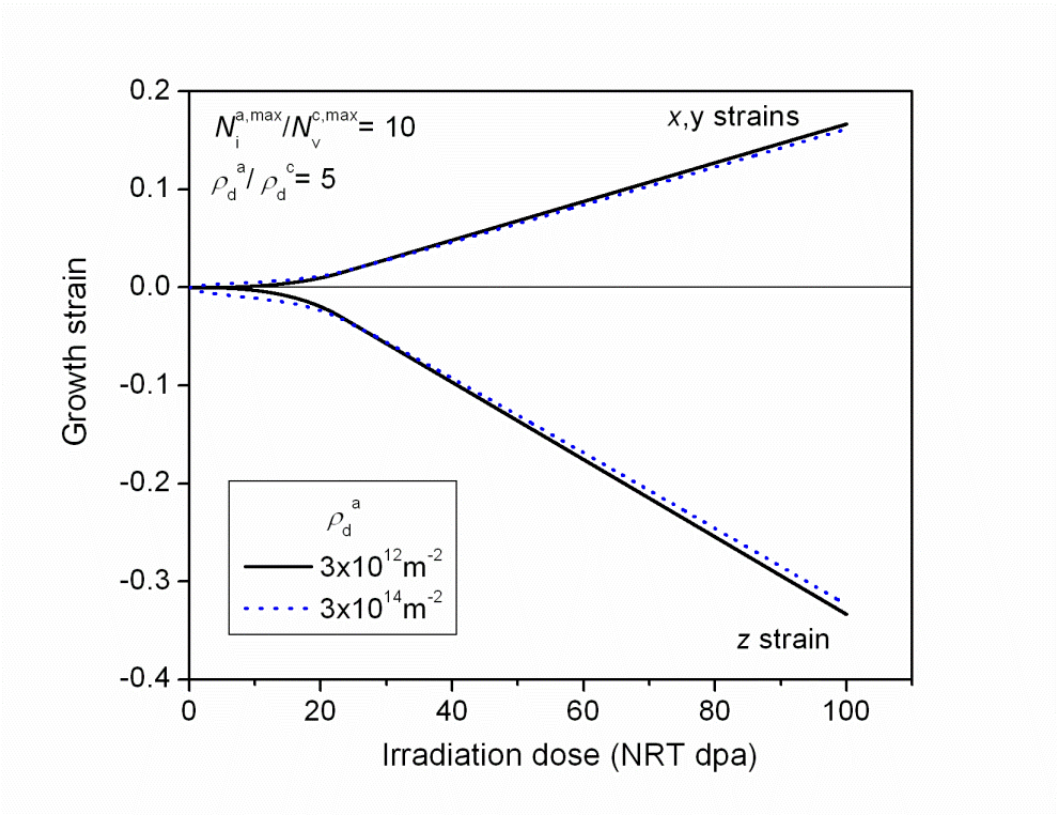
$N_i^{a,max}/N_v^{c,max}$ = 10
ρ_d^a/ρ_d^c = 5
x,y strains
z strain
ρ_d^a
3x10^{12}m^{-2}
3x10^{14}m^{-2}
Growth strain
Irradiation dose (NRT dpa)
0.2
0.1
0.0
-0.1
-0.2
-0.3
-0.4
0
20
40
60
80
100

Fig. 8.

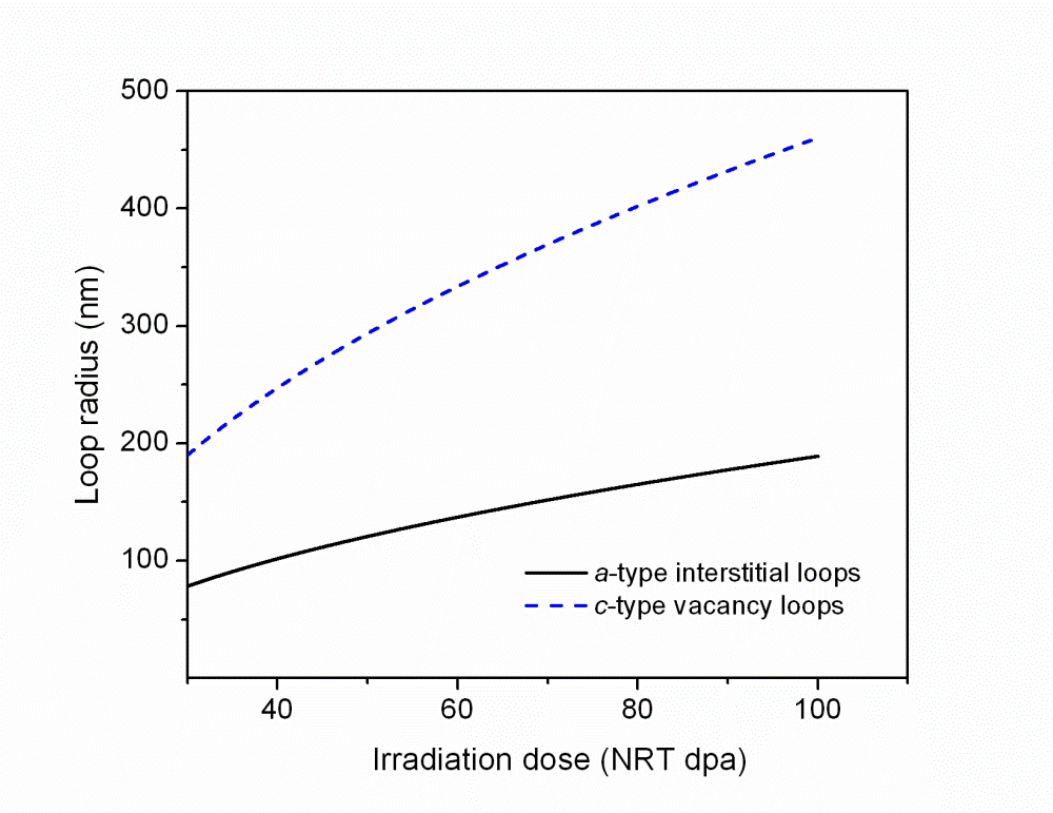
500
400
300
200
100
Loop radius (nm)
40
60
80
100
Irradiation dose (NRT dpa)
a-type interstitial loops
c-type vacancy loops

Fig. 9.

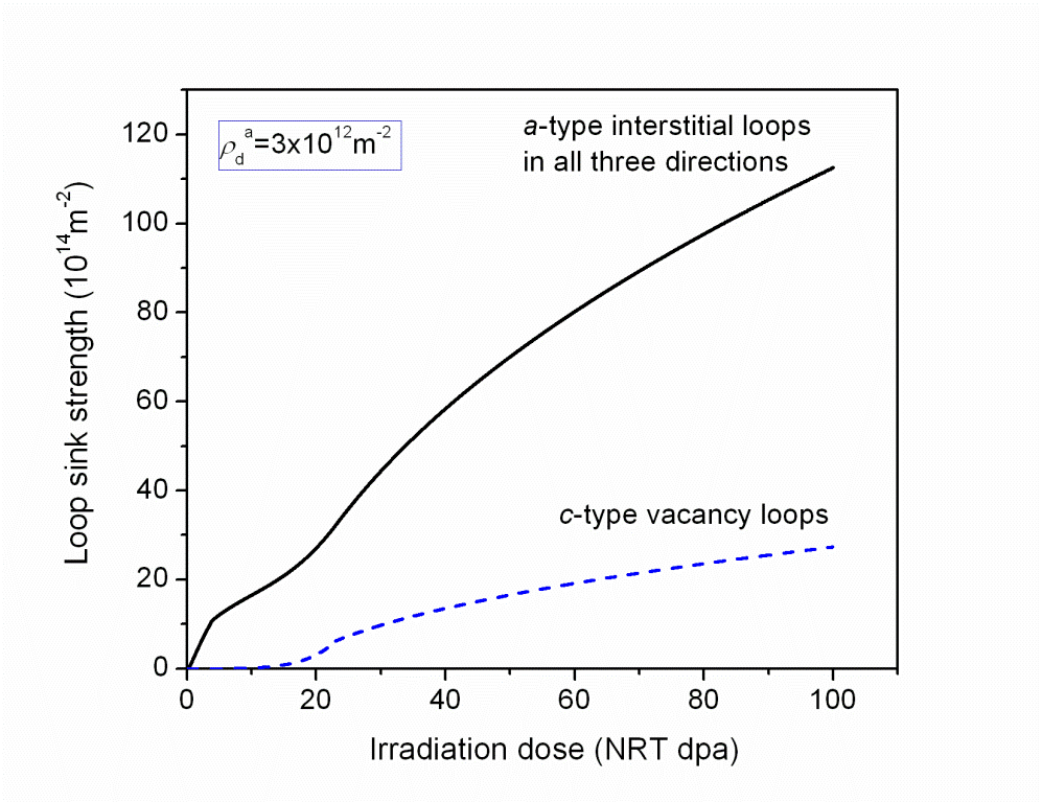
ρ_d^a=3x10^{12}m^{-2}
a-type interstitial loops
in all three directions
c-type vacancy loops
Loop sink strength (10^{14}m^{-2})
Irradiation dose (NRT dpa)
0
20
40
60
80
100
120

Fig. 10.

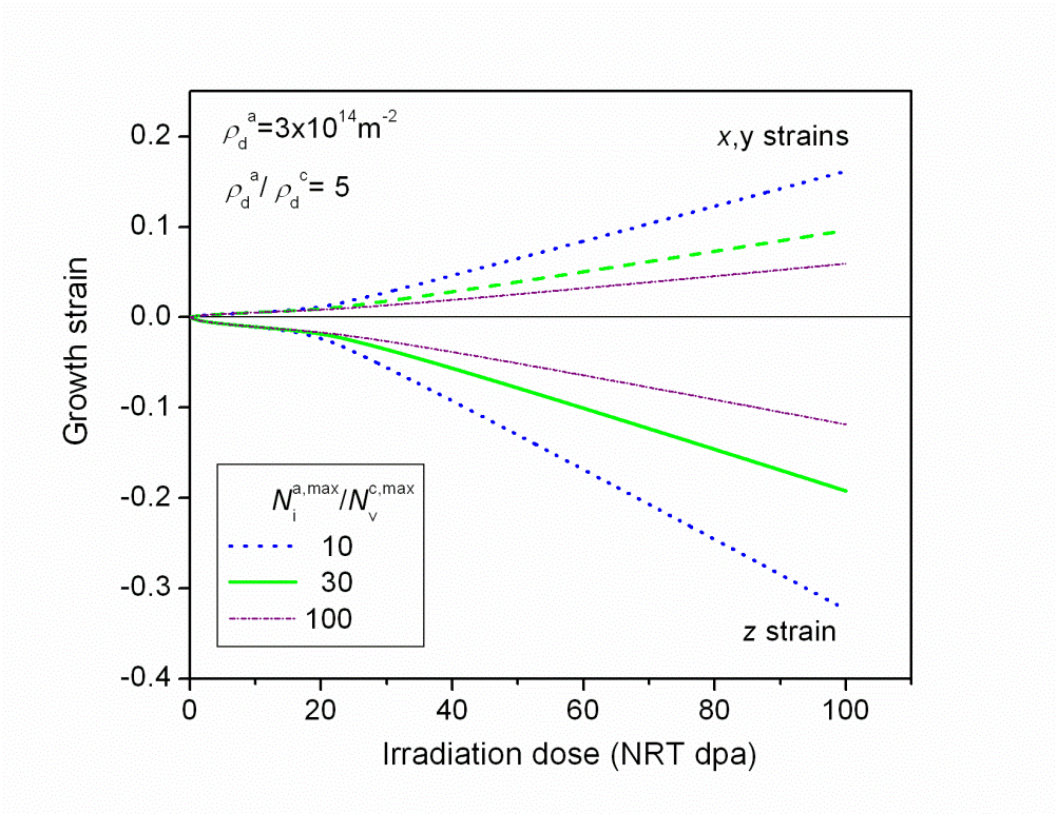
ρ_d^a=3x10^{14}m^{-2}
ρ_d^a/ ρ_d^c= 5
x,y strains
z strain
$N_i^{a,max}/N_v^{c,max}$
10
30
100
Growth strain
Irradiation dose (NRT dpa)
0.2
0.1
0.0
-0.1
-0.2
-0.3
-0.4
0
20
40
60
80
100

Fig. 11.

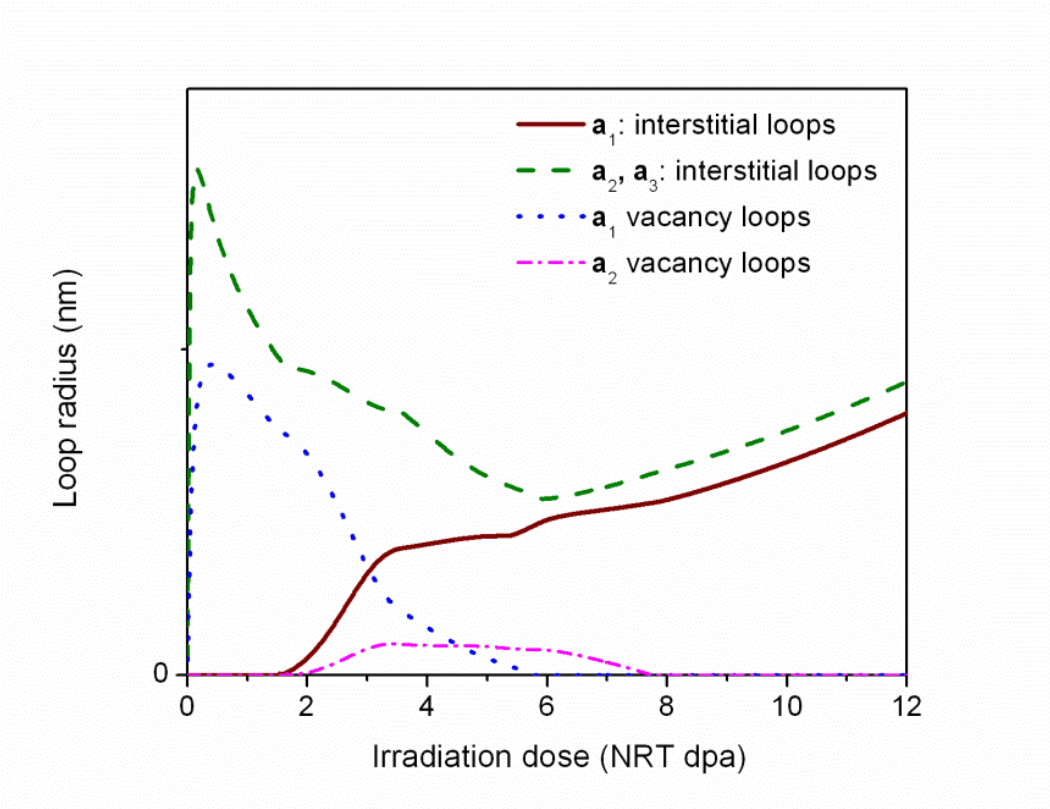
a1: interstitial loops
a2, a3: interstitial loops
a1 vacancy loops
a2 vacancy loops
Loop radius (nm)
0
0
2
4
6
8
10
12
Irradiation dose (NRT dpa)

Fig. 12.

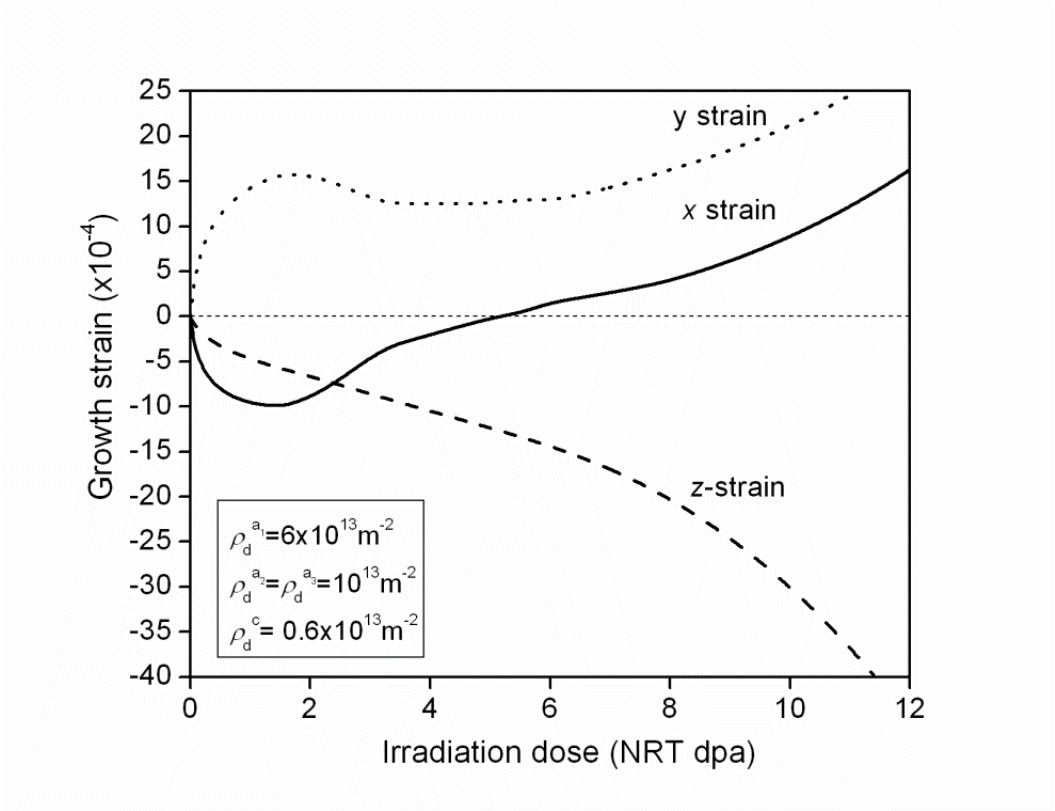
y strain
x strain
z-strain
Growth strain (x10^-4)
Irradiation dose (NRT dpa)
ρd^a1=6x10^13m^-2
ρd^a2=ρd^a3=10^13m^-2
ρd^c= 0.6x10^13m^-2
25
20
15
10
5
0
-5
-10
-15
-20
-25
-30
-35
-40
0
2
4
6
8
10
12

Fig. 13.

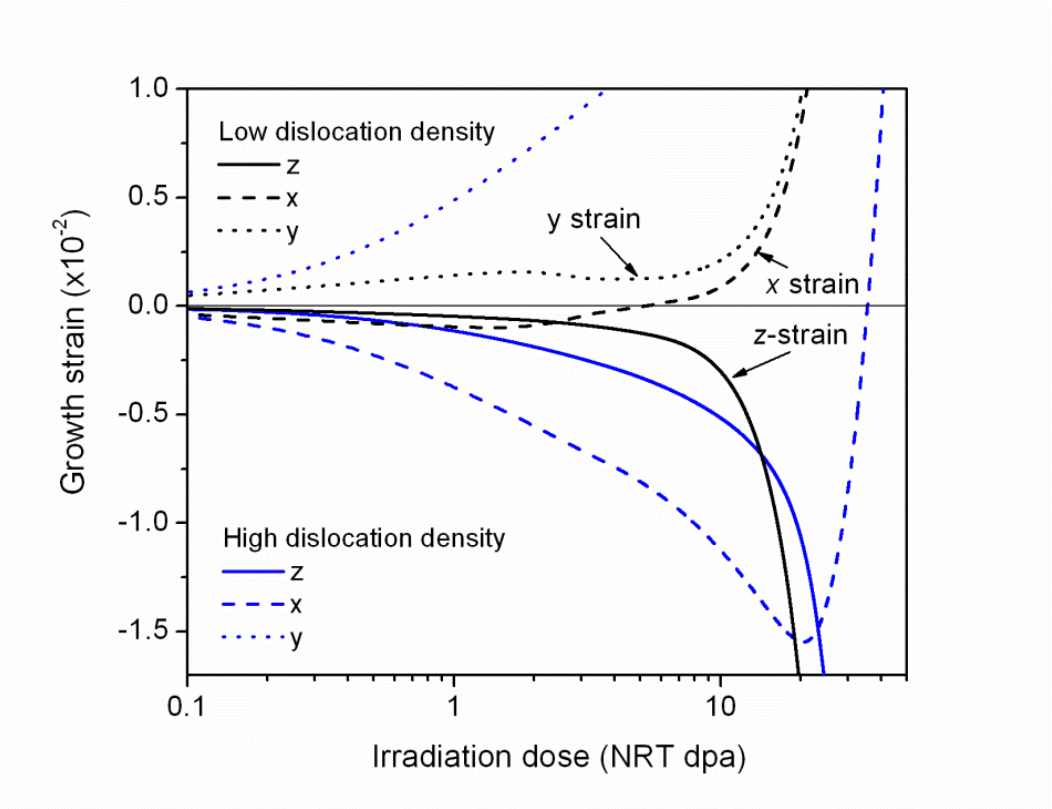
Low dislocation density
z
x
y
y strain
x strain
z-strain
High dislocation density
z
x
y
Growth strain (x10^{-2})
1.0
0.5
0.0
-0.5
-1.0
-1.5
0.1
1
10
Irradiation dose (NRT dpa)

Fig. 14.

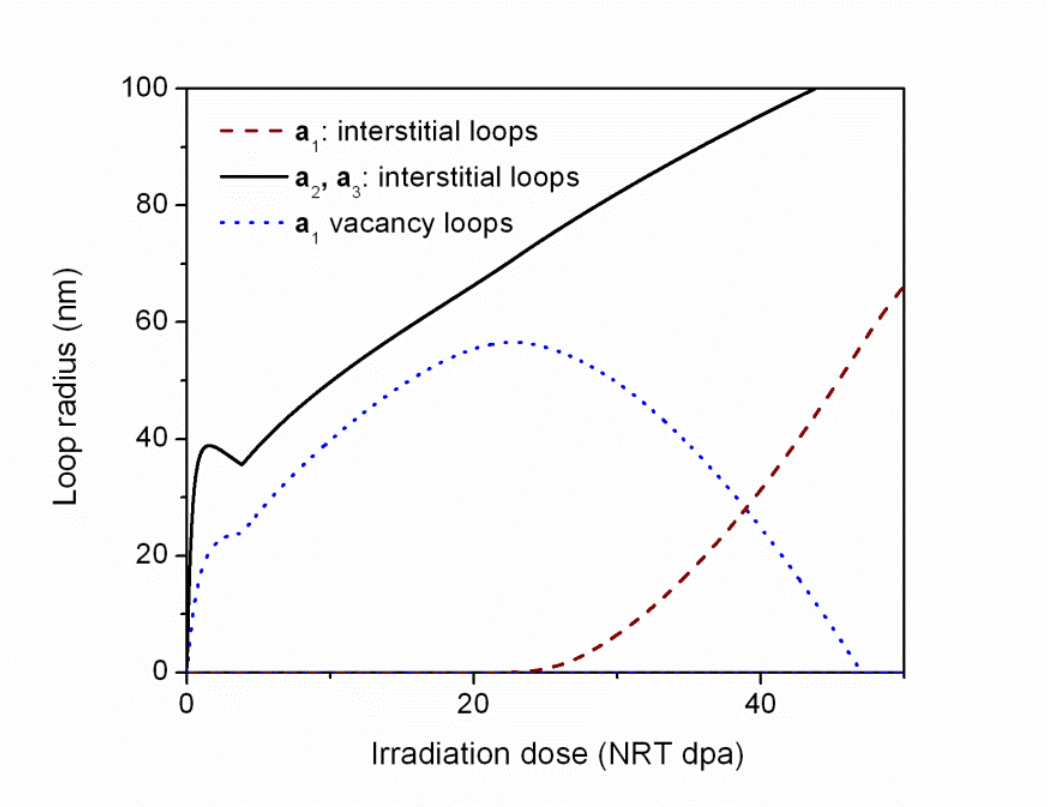
100
80
60
40
20
0
0
20
40
Loop radius (nm)
Irradiation dose (NRT dpa)
a1: interstitial loops
a2, a3: interstitial loops
a1 vacancy loops

Fig. 15.

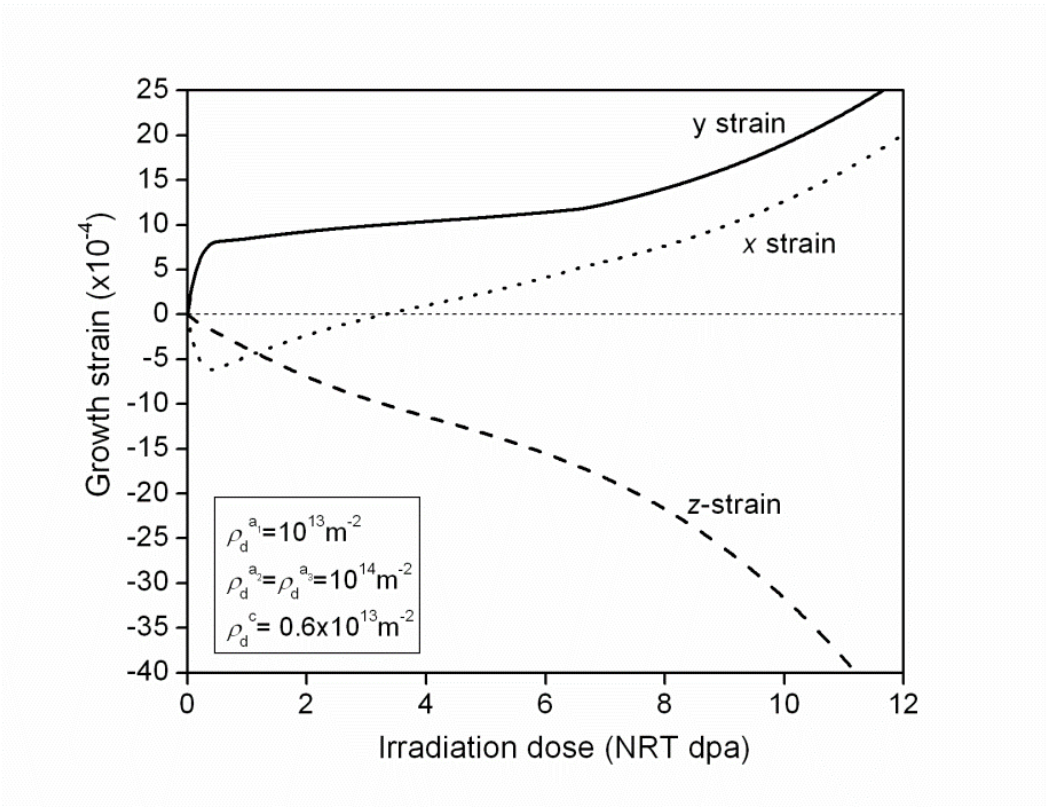
y strain
x strain
z-strain
Growth strain (x10^-4)
Irradiation dose (NRT dpa)
ρd^a1=10^13m^-2
ρd^a2=ρd^a3=10^14m^-2
ρd^c= 0.6x10^13m^-2
25
20
15
10
5
0
-5
-10
-15
-20
-25
-30
-35
-40
0
2
4
6
8
10
12

Fig. 16.

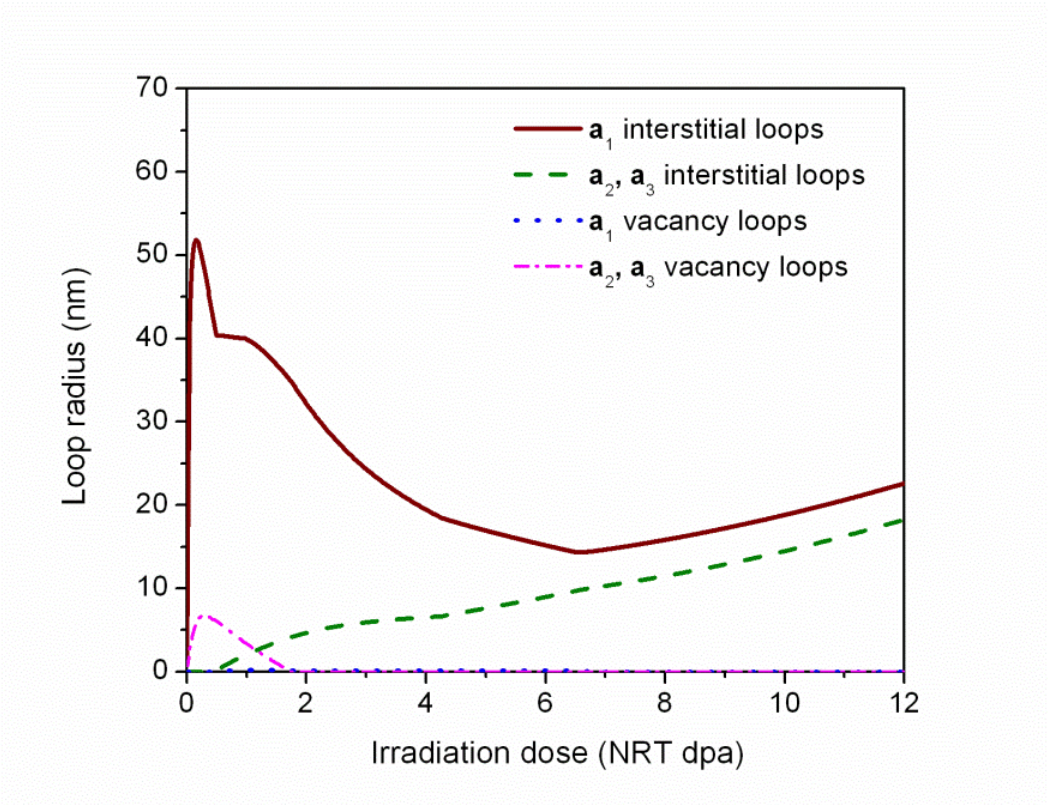
70
60
50
40
30
20
10
0
Loop radius (nm)
0
2
4
6
8
10
12
Irradiation dose (NRT dpa)
a1 interstitial loops
a2, a3 interstitial loops
a1 vacancy loops
a2, a3 vacancy loops

Fig. 17.

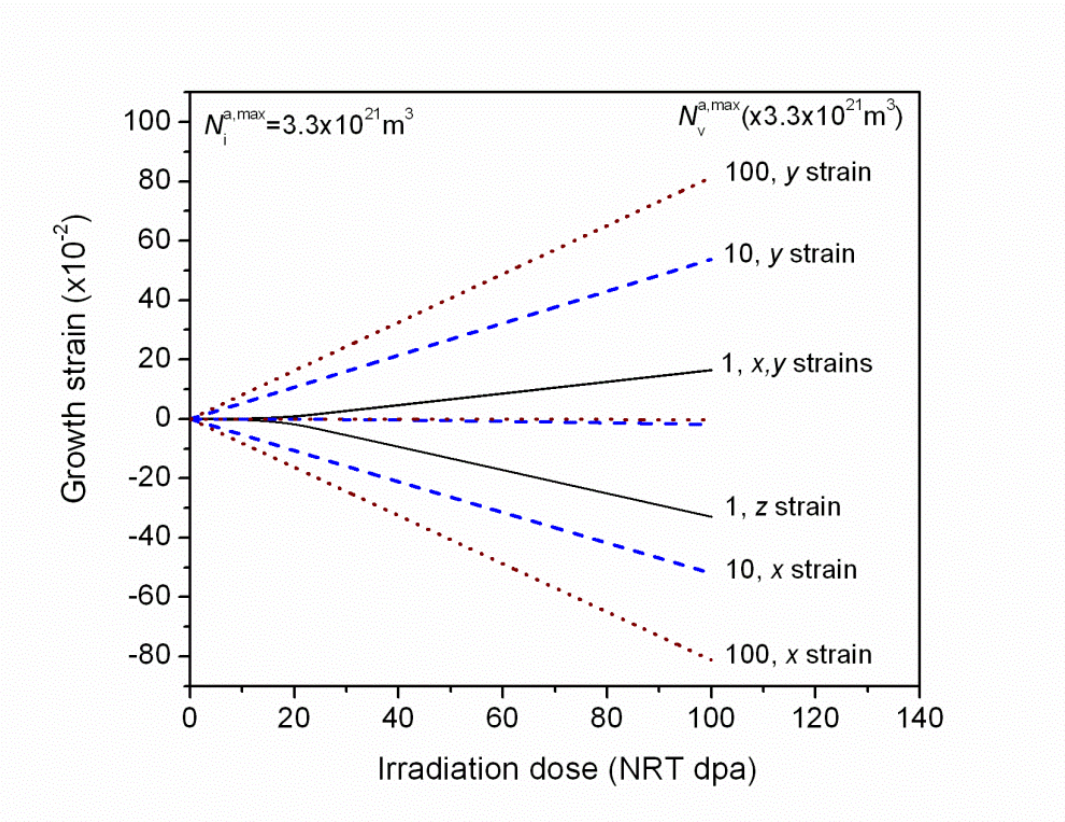
$N_i^{a,max}$=3.3x10^{21}m^3
$N_v^{a,max}$(x3.3x10^{21}m^3)
100, *y* strain
10, *y* strain
1, *x*,*y* strains
1, *z* strain
10, *x* strain
100, *x* strain
Growth strain (x10^{-2})
Irradiation dose (NRT dpa)
100
80
60
40
20
0
-20
-40
-60
-80
0
20
40
60
80
100
120
140

Fig. 18.

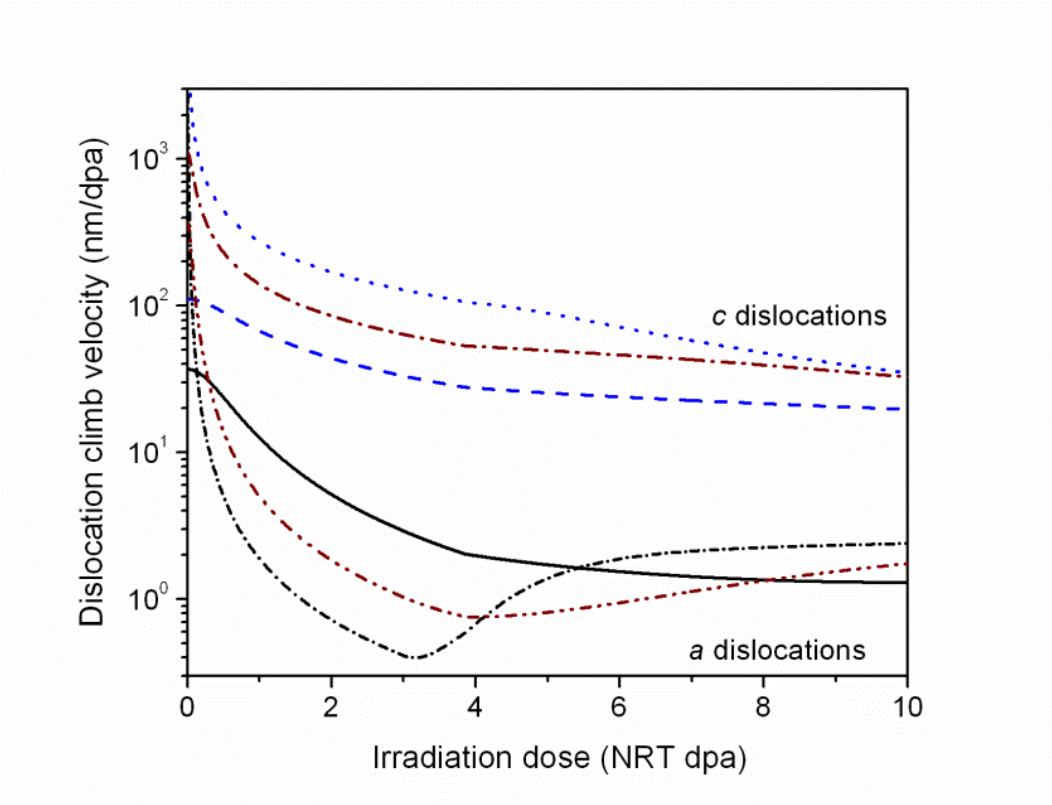

Fig. 18. Dislocation climb velocities at small irradiation doses for *c* dislocations (dotted, blue – dislocation density 10^{12} m^{-2}; dash dot, wine – 10^{13}; dash, blue – 10^{14}) and *a* dislocations (dot dash dot, black – 10^{12}; dash dot dot, wine – 10^{13}; solid, black – 10^{14}).

Fig. 19.

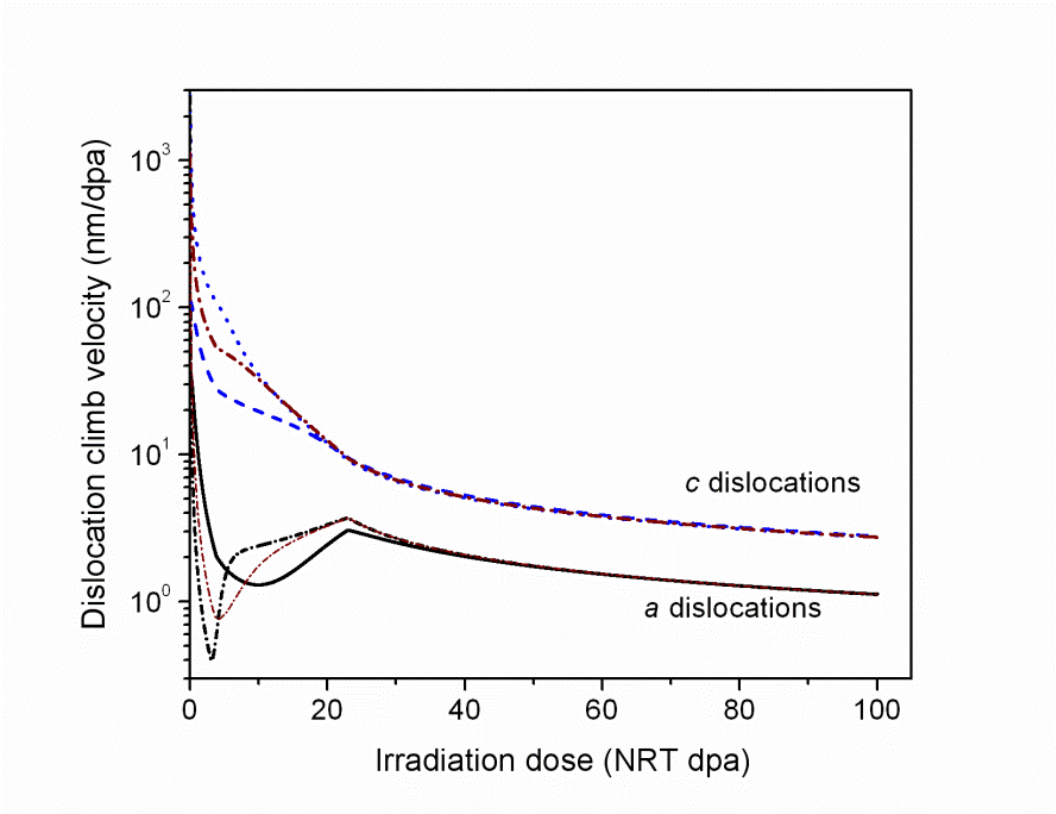
Dislocation climb velocity (nm/dpa)
10^3
10^2
10^1
10^0
c dislocations
a dislocations
0
20
40
60
80
100
Irradiation dose (NRT dpa)
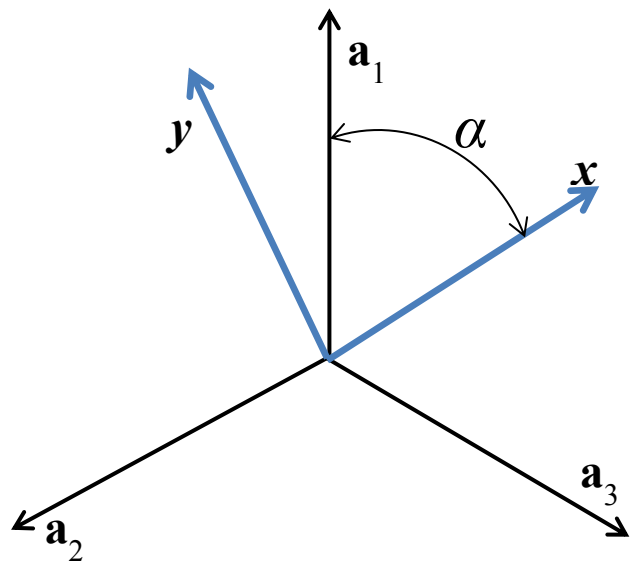
Fig. 20.